

Review

Nanostructured Oxides Synthesised via $scCO_2$ -Assisted Sol-Gel Methods and Their Application in Catalysis

Yehan Tao and Paolo P. Pescarmona * 

Chemical Engineering Group, Engineering and Technology Institute Groningen (ENTEG), University of Groningen, Nijenborgh 4, Groningen 9747, The Netherlands; y.h.tao@rug.nl

* Correspondence: p.p.pescarmona@rug.nl; Tel: +31-50-363-6521

Received: 2 April 2018; Accepted: 9 May 2018; Published: 17 May 2018



Abstract: Nanostructured metal oxides and silicates are increasingly applied in catalysis, either as supports or as active species in heterogeneous catalysts, owing to the physicochemical properties that typically distinguish them from bulk oxides, such as higher surface area and a larger fraction of coordinatively unsaturated sites at their surface. Among the different synthetic routes for preparing these oxides, sol-gel is a relatively facile and efficient method. The use of supercritical CO_2 ($scCO_2$) in the sol-gel process can be functional to the formation of nanostructured materials. The physical properties of the $scCO_2$ medium can be controlled by adjusting the processing temperature and the pressure of CO_2 , thus enabling the synthesis conditions to be tuned. This paper provides a review of the studies on the synthesis of oxide nanomaterials via $scCO_2$ -assisted sol-gel methods and their catalytic applications. The advantages brought about by $scCO_2$ in the synthesis of oxides are described, and the performance of oxide-based catalysts prepared by $scCO_2$ routes is compared to their counterparts prepared via non- $scCO_2$ -assisted methods.

Keywords: nanostructured oxides; supercritical CO_2 ; sol-gel; catalysis

1. Introduction

1.1. Nanostructured Oxides and Their Synthesis

Metal oxides and silicates draw great research attention for their wide range of applications in catalysis [1]. Various oxides are commercially available as both catalytically active materials (e.g., TiO_2 [2], NiO [3], Fe_2O_3 [4], ZnO [5], Cr_2O_3 [6], Co_3O_4 [7], WO_3 [8]) and as supports for nanoparticles (e.g., SiO_2 [9], TiO_2 [10], Al_2O_3 [11]), with applications in chemical and pharmaceutical industries. Decreasing the size of the oxide particles to the nanoscale or generating porosity in the nanometre range can be beneficial for catalytic applications. Namely, nanostructuring of the oxides brings about an intrinsic increase in the surface-to-volume ratio and, thus, in the specific surface area. The surface of nanomaterials is also rich in coordinatively unsaturated sites (CUS) that can act as catalytic sites [12]. This combination of features is highly desirable in catalytic applications. Therefore, it is valuable to develop synthesis methods that can promote the controlled formation of nanostructured oxides—ideally with the possibility of tuning the surface area, the porosity, the particle size and distribution, the crystallinity and the composition—while at the same time being affordable, energy efficient and environmentally friendly.

Until now, a variety of methods have been developed for the synthesis of nanostructured metal oxides and silicates [1], including sol-gel methods, template techniques, hydrothermal or solvothermal routes, precipitation methods, chemical vapour deposition (CVD), laser ablation and electrochemical

methods. It should be pointed out that some of these approaches can be combined in one synthesis process. For instance, in the preparation of widely studied mesoporous materials as MCM-41 and SBA-15 silicates, sol-gel, template, hydrothermal and solvothermal methods are combined [13]. On the other hand, these synthesis methods are not devoid of drawbacks. For example, the template technique requires calcination at high temperature (typically ≥ 400 °C) to remove the organic surfactants which are used as templates (e.g., cetyl trimethylammonium bromide (CTAB) or Pluronic 123). Besides the high cost of the surfactants, a drawback of this method is the tendency of the materials to undergo shrinkage and (partial) collapse of the original structure during the thermal treatment, which in turn can greatly reduce the catalytic activity. CVD and laser ablation methods suffer from instability of raw materials under the operating conditions, abundant energy consumption, and costly purification steps [1]. Compared to the other methods, sol-gel routes benefit from straightforward and generally inexpensive synthesis conditions and a high degree of versatility [14,15]. The formation of nanostructured oxides with sol-gel methods can be promoted by using supercritical CO₂ (scCO₂) as a reaction medium or as a drying agent. This review focuses on the use of such scCO₂-assisted sol-gel methods for the synthesis of metal oxides and silicates finding application in heterogeneous catalysis.

1.2. Sol-Gel Method

The sol-gel method is a widely-used synthesis approach for the preparation of inorganic (nano) materials. Advantages of the sol-gel method include its tolerance to precursor variation, mild reaction conditions and easy scale-up. A broad range of nanostructured metal oxides, silicates, and their composites has been successfully obtained through sol-gel methods [15–18], ranging from nanoparticles, nanorods, nanofibres or nanotubes, to materials with pores in the nanoscale, which can be subdivided in microporous (pore diameter, $d_p < 2$ nm), mesoporous ($2 \text{ nm} \leq d_p \leq 50$ nm) and macroporous ($d_p > 50$ nm) materials.

The process of sol-gel synthesis typically starts with a hydrolysis and condensation step leading to the formation of a colloidal solution (sol). Upon further condensation, the sol evolves into an integrated network (gel), in the voids/pores of which solvent molecules are trapped. The gelation is generally followed by aging and drying (Figure 1). During the aging step, consolidation of the structure is achieved through the continuation of the condensation reactions. The gel can be converted into the final solid oxide product by removing the solvent through washing, drying and/or thermal treatment.

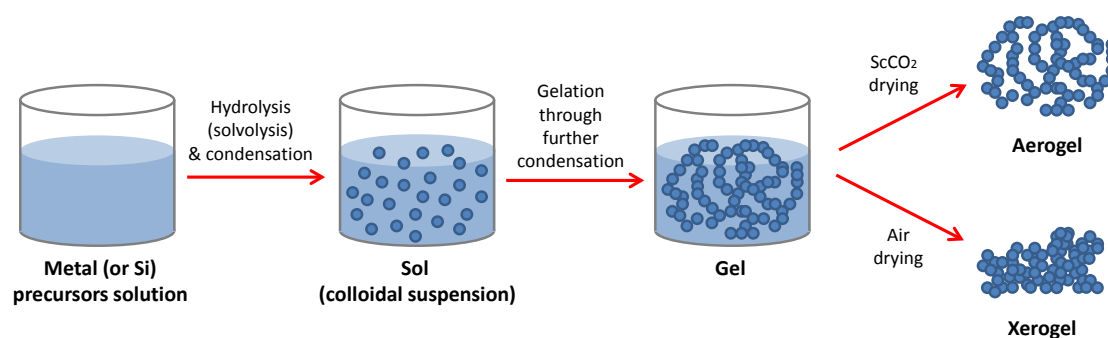


Figure 1. General scheme of a sol-gel synthesis method.

The initial hydrolysis and condensation of the metal or silicon precursors (typically alkoxides or chlorides) can occur sequentially or in a concerted step. The nature of the species formed at this stage is determined by the element and ligand constituting the metal or silicon precursor, by its concentration, the pH, the solvent and the remaining reaction conditions [19,20]. For several metal precursors, this hydrolysis and condensation step leads to the formation (nucleation) of nanoparticles with a defined size. Such particles can behave as a colloid, thus constituting the sol. The formed

particles can undergo further growth through Ostwald ripening and aggregate to generate the network of the gel [19].

It is important to note that the sol-gel synthesis can be carried out also in non-aqueous media. In such case, the solvolysis and condensation step proceed through the reaction of the metal precursors with oxygen-donors other than water (e.g., alcohols, alkoxides, carboxylic acids, carboxylates), though H₂O can form in situ during the process [17].

It should be mentioned that for the formation of mixed oxides, the difference in rates of hydrolysis (solvolysis) and condensation between different precursors can affect the formation of the desired products (i.e., determining whether a homogeneous dispersion of two species can form). In such cases, strategies to compensate these differences have been developed, such as pre-hydrolysis of the precursors with lower hydrolysis rate (e.g., silicon alkoxides) or introduction of selected chelating ligands that slow down the hydrolysis of metal precursors with higher hydrolysis rate (e.g., main group and transition group metal alkoxides) [20].

Sol-gel chemistry often offers the possibility to control the morphology and physicochemical properties of the products by adjusting the synthesis parameters (such as the type and concentration of precursors, the nature of the solvent, the amount and addition rate of H₂O or other oxygen-donors, the temperature, the presence and type of condensing agent and the drying methodology). The properties that can be tailored by tuning the sol-gel synthesis include the particle size, dispersion and morphology; the porosity (pore volume, size and distribution); the surface area and surface polarity; the crystallinity; the number and strength of acid and base sites. However, the conventional sol-gel method presents some limitations. The hydrolysis and condensation step is hard to control when the synthesis involves more than one metal precursor. Besides, the relatively high viscosity and surface tension of most solvents used in sol-gel methods imply that the solvent molecules cannot readily diffuse into the pores of the formed nanostructured network, thus hindering the formation of a homogeneous pore structure and pore dispersion. Moreover, the subsequent drying by thermal treatment to evaporate the residual solvent molecules leads to large capillary forces in the small pores, which tend to cause shrinkage and a partial or full collapse of the structure with a drastic reduction of surface area and porosity. These drawbacks can be tackled by employing supercritical CO₂ as the reaction medium and/or drying agent, exploiting its low viscosity and surface tension, its straightforward removal and the possibility to tune its properties by adjusting the operating temperature and CO₂ pressure. Additionally, scCO₂ is an environmentally benign solvent. The properties of supercritical CO₂ are described in more detail in the following section.

1.3. Supercritical CO₂ and its Properties as Reaction Medium and Drying Agent

Supercritical CO₂ is defined as carbon dioxide at temperature and pressure above its critical point [$T_C = 304.25$ K (31.1 °C); $p_c = 7.39$ MPa (73.9 bar or 72.9 atm)]. These values indicate that the supercritical state of CO₂ is accessible at relatively mild conditions (Figure 2). Above the critical point, there is no phase boundary between gas and liquid phases and the fluid has thus intermediate properties between those of gas and liquid. The viscosity of scCO₂ (between 10^{-5} and 10^{-4} Pa/s) is similar to that of gases (10^{-5} to 3×10^{-5} Pa/s), whereas its density (0.1 to 1 g/cm³) is close to that of liquids (0.6 to 1.6 g/cm³) and its diffusivity (10^{-4} to 10^{-3} cm²/s) is intermediate between that of liquids ($<10^{-5}$ cm²/s) and gases ($\sim 10^{-1}$ cm²/s). These physical properties can be easily tuned by changing the temperature and pressure of CO₂, with an increase of pressure at constant temperature leading to higher density and a more liquid-like behaviour and an increase in temperature at constant pressure leading to a lower density and a more gas-like behaviour. Moreover, the pressurisation and depressurisation rate can be controlled. ScCO₂ has been widely employed in a large range of applications including selective extraction, exfoliation and intercalation of layered materials, cleaning and drying reaction residues in meso- and microporous materials, impregnation or encapsulation of nanoparticles into polymers and inorganic substrates, and materials synthesis. Several comprehensive reviews on the synthesis of nanomaterials in scCO₂ have been published [14,21–27]. In this review,

we provide an overview of the specific application of scCO₂ in the synthesis of nanostructured metal oxides and silicates employed in heterogeneous catalysis.

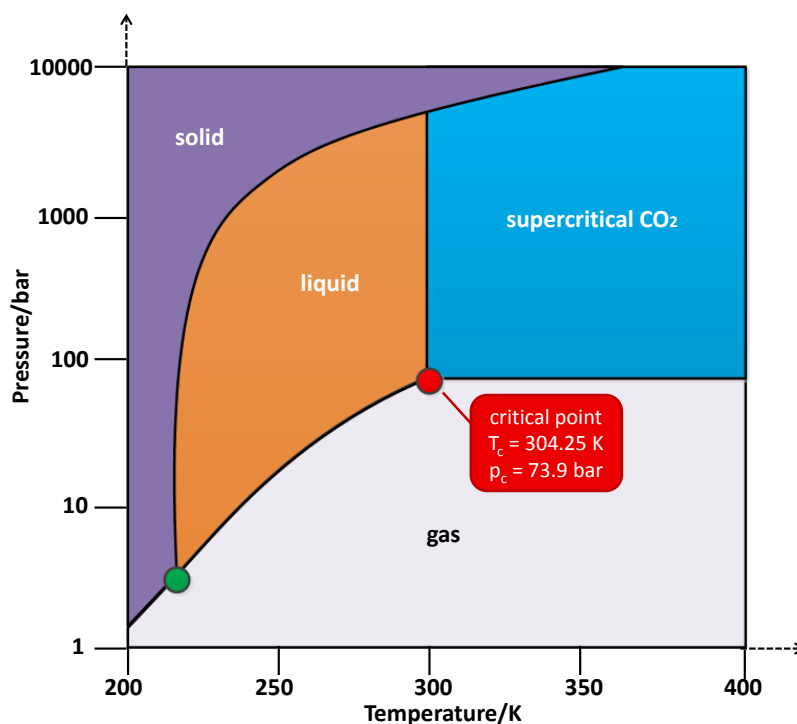


Figure 2. Phase diagram of CO₂.

ScCO₂ possesses several advantageous properties when used in the synthesis of nanomaterials [21–23,27]. Firstly, the solvating ability of scCO₂ is a function of its density, which increases with pressure at constant temperature. In general, non-polar compounds are soluble in scCO₂ because CO₂ is a relatively non-polar compound (dipole moment, $\mu = 0$; dielectric constant, $\epsilon_r = 1.1\epsilon_0$ at 353 K, 100 bar). Moreover, polar compounds with hydroxyl, carbonyl, chloride or fluoride groups can be dissolved to a certain extent in scCO₂ due to the large quadrupole moment of CO₂ and to the polarity of the C=O bonds. This means that both non-polar and polar compounds can be dissolved in scCO₂, though it should be noted that solubilities in scCO₂ are lower than in the appropriate organic solvents for each class of compounds. This feature can prove beneficial for those synthesis processes involving both polar and non-polar precursors (see Section 2.1 where the use of scCO₂ as the solvent for the synthesis of oxides is discussed). The solvating ability of scCO₂ can be further increased by the introduction of co-solvents, among which the most commonly used are alcohols, acetone, hexane, formic acid and acetic acid. For example, the water used in the hydrolysis step of sol-gel methods and scCO₂ can form a single phase with the assistance of alcohol as co-solvent. In such cases, the supercritical point of the mixture is different from that of pure CO₂, and under certain temperatures and pressures, the resulting solution can also reach a supercritical status. ScCO₂ is completely miscible with gases while gases are only sparingly soluble in organic solvents. Therefore, significantly high gas concentration can be achieved in the scCO₂ phase, which is advantageous for reactions involving both gas and liquid reactants. This enhanced miscibility of reactants in scCO₂ can greatly eliminate interphase transport limitations in multiphase reactions, leading to a higher mass transfer rate of the reactants.

Another asset of scCO₂ is its high diffusivity compared to liquid solvents, which means that scCO₂ can readily penetrate through porous matrices. This feature is very important for syntheses by impregnation methods (see Section 2.1) but also for removal of molecules from pores in scCO₂ drying (see Section 2.3). The high diffusivity of scCO₂ also allows the rapid expansion of a solution when this

is injected into a scCO₂ medium. This feature is exploited in the application of scCO₂ as anti-solvent for the synthesis of nanomaterials (see Section 2.2).

Importantly, reactions involving scCO₂ allow the straightforward separation of the synthesised materials from the CO₂ by depressurisation, upon which CO₂ returns to the gas phase and gets removed from the solid with maximum preservation of the formed structure of the material. The surface tension of scCO₂ is negligible, which differentiates it from water and organic solvents. This is a crucial feature for the use of scCO₂ as the drying agent for gels (see Section 2.3). In the scCO₂ drying process, scCO₂ diffuses into the pores of the gel and dissolves the organic solvent trapped therein. Continuous flushing with scCO₂ allows efficient removal of the organic solvent. Then, the scCO₂ present in the structure can be easily removed by depressurisation, with minimum effect (shrinkage/collapse) on the pore architecture as a consequence of the negligible surface tension of scCO₂. Afterwards, the CO₂ can be easily recovered and reused for the next synthesis round. Finally, it is worth mentioning that CO₂ is significantly less harmful than the majority of organic solvents employed in the synthesis of materials and can be thus considered as a green solvent.

2. Nanostructured Oxides Synthesised via scCO₂-Assisted Sol-Gel Methods

The utilisation of scCO₂ in the sol-gel synthesis of nanostructured metal oxides and silicates can be divided into three categories: the use of scCO₂ as a solvent, as anti-solvent and as a drying agent. Each of these approaches is reviewed in detail in the following sections. It should be pointed out that the synthetic routes that will be discussed are not limited to the typical sol-gel synthesis in which macroscopic sol or gel intermediates are formed, but also include other synthesis methods based on hydrolytic condensations in which metal oxide precipitates are formed but no obvious formation of sol or gel is observed.

2.1. ScCO₂ as Solvent

The advantages of scCO₂ discussed in Section 1.3 (e.g., tuneable dissolving power and density and high diffusivity) make it a promising solvent in sol-gel processes for the production of nanostructured metal oxides and silicates, as the starting precursors are directly dissolved in scCO₂. At the end of the sol-gel process, the CO₂ can be easily removed from the products by straightforward depressurisation. This feature is beneficial to preserve the porous structure and surface area formed during the sol-gel process, which are two crucial parameters for catalytic applications. In 1997, Loy et al. reported the direct sol-gel polymerisation of alkoxysilane monomers in scCO₂ to produce SiO₂ [28]. From then on, a variety of oxides have been successfully prepared directly using sol-gel methods in scCO₂, including single metal oxides, mixed oxides, doped metal oxides, oxide/metal nanoparticle composites as well as oxide/polymer composites (Table 1). The morphology of these oxides ranges from spherical nanoparticles to nanotubes, nanorods, nanofibres/nanowires or nanosheets. Charpentier's group published a series of articles about sol-gel synthesis in scCO₂ of Al₂O₃ [11], SiO₂ [29,30], (doped) TiO₂ [10,29,31], ZrO₂ [29], and oxide-containing composites [32–37]. An example of the reactor set-up used for these syntheses is presented in Figure 3. In a typical protocol, the metal (or Si) precursors, other reactants, and solvents (Table 1) were mixed in the autoclave. Then, the reactor was heated and pressurised to the chosen scCO₂ conditions for a selected time. Afterwards, CO₂ was removed by depressurisation and the resulting solid product was further dried and optionally calcined. The whole sol-gel process in scCO₂ could be monitored by FTIR spectroscopy with an in-situ probe and by online gas chromatography–mass spectrometry (GC-MS) analysis [36].

Table 1. Summary of methods for the direct sol-gel synthesis of nanostructured metal oxides (and silica) in scCO₂.

Product	Morphology	Precursors, Reactants, Co-Solvents	Ref.
TiO ₂	Aerogel	Titanium (IV) isopropoxide (TIP), acetic acid	[29]
	Nanoparticles	TIP, deionised water, polypropylene fibre	[38]
	Spherical particles, micron-size rods, nanofibres	TIP, Titanium butoxide (TBO), acetic acid	[10]
	Spherical particles	Diisopropoxititanium bis(acetylacetonate) (DIPBAT), absolute ethanol, isopropyl alcohol	[2]
SiO ₂	Molecular sieve membranes	Tetraethyl orthosilicate (TEOS), ultrapure water, 2-propanol, nitric acid, yttrium (III) acetate hydrate.	[39]
	Aerogel	TEOS, acetic acid	[29]
	Nanoparticles	Tetramethyl orthosilicate (TMOS), TEOS, acetone, benzoic acid, acetic acid, formic acid, water	[30]
	Ordered porous structure	TEOS, water, polystyrene latex	[9]
ZrO ₂	Aerogel	Zirconium butoxide (ZBO), acetic acid	[29]
Al ₂ O ₃	Nanofibres	Aluminium (III) isopropoxide (AIP), acetic acid	[11]
Pd-SiO ₂	Nanoparticles	TMOS, formic acid, polydimethylsiloxane (PDMS), palladium(<i>N,N'</i> -bis(1,1,1,3,5,5,5)heptafluoro-2,4-pentanediiiminate (Pd(II)HFDPDI)	[40]
N- and N/Zr-doped TiO ₂	Nanofibres and flake-like structures	TIP, zirconium (IV) propoxide (ZPO), acetic acid, isopropanol, triethylamine	[32]
Fe-doped TiO ₂ /rGO	Nanowires	TIP, iron chloride, acetic acid, reduced graphite oxide (rGO)	[31]
ZrO ₂ -TiO ₂	Nanotubular structures	TIP, ZPO, acetic acid	[33]
	Nanotubes	TIP, ZPO, acetic acid	[34]
	Nanotubes	TIP, ZPO, acetic acid	[35]
Y-ZrO ₂	Spherical nanoparticles	Zirconium hydroxyacetate, yttrium acetate, pentane or 2-propanol, nitric acid	[41]
TiO ₂ -SiO ₂	Nanostructured composites	TMOS, TIP, formic acid, Pluronic 17R4 surfactant	[42]
	Spherical or cubic nanoparticles	Tetrabutyl titanate, TEOS, polyethylene glycol (PEG) 20000, aqueous ammonia, ethanol	[43]
SiO ₂ /polyethylene	Polymer/SiO ₂ nanocomposites	TMOS, TEOS, acetic acid, polyethylene	[36]
Hydroxyapatite-TiO ₂	Nanocomposites	Calcium nitrate tetrahydrate, diammonium hydrogen phosphate, CTAB, PEG 400, TIP, glacial acetic acid, ammonium hydroxide, dichloromethane, ethanol, polycaprolactone	[37]

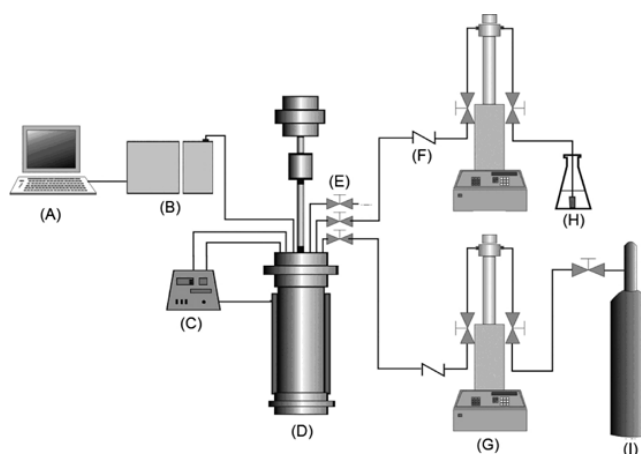


Figure 3. Schematic representation of the experimental set-up for the synthesis of materials in $scCO_2$: (A) computer; (B) online GC-MS; (C) temperature and RPM controller with pressure display; (D) 100-mL autoclave equipped with a diamond FTIR probe; (E) needle valves; (F) check valves; (G) syringe pump; (H) supply for liquid reactants/solvents, and (I) CO_2 cylinder. (Reprinted with permission from [36]. Copyright American Chemical Society, 2009).

The use of $scCO_2$ as the solvent for the synthesis of nanostructured oxides was also applied using a high-throughput unit for performing reactions in $scCO_2$ (Figure 4) [42]. The reported set-up consisted of four modules: a visualisation batch reactor, a block with 10 parallel batch reactors, a block with 24 parallel batch reactors and a fixed-bed reactor. All the batch reactors were individually stirred. The four modules could be used simultaneously. Check valves protected against backflow thus preventing contamination between the single batch reactors. This high-throughput unit enabled the rapid preparation of a series of TiO_2 - SiO_2 composite materials while granting the same conditions of pressure and temperature in each batch reactor. The synthesis was carried out in a $scCO_2$ /formic acid medium in which the role of the formic acid was to balance the rate of the hydrolysis and condensation of the silicon and titanium alkoxide precursors. At the start of the preparation, the chosen amounts of $Ti(OPr^i)_4$, $Si(OMe)_4$ and surfactant (Pluronic 17R4) were dosed into a Teflon liner and preheated at $35\text{ }^\circ\text{C}$. Formic acid was added prior to closing the block. The reactor was pressurised at 85 bar with CO_2 and subsequently heated to $75\text{ }^\circ\text{C}$. The powders obtained after depressurisation were calcined at $350\text{ }^\circ\text{C}$ and then were employed as photocatalysts for the degradation of pollutants (see Section 3.1).

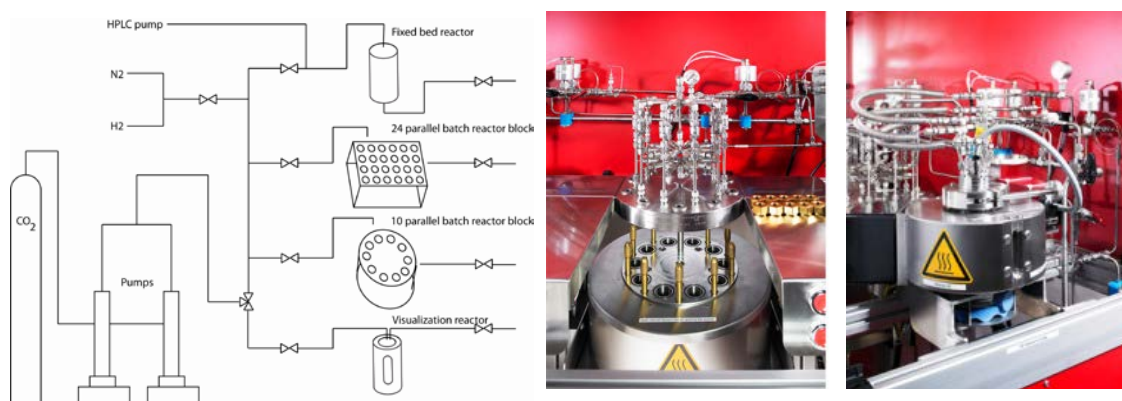


Figure 4. From left to right: schematic overview of the high-throughput $scCO_2$ unit used to prepare the TiO_2 - SiO_2 composites; reactor block with 10 batch reactors; visualisation reactor used to monitor the phase behaviour during the synthesis. (Adapted with permission from [42]. Copyright Wiley-VCH, 2011).

The high-diffusivity of scCO_2 is also exploited in deposition methods in which precursors dissolved in the scCO_2 phase are impregnated and then precipitated inside the pores of a selected material (e.g., mesoporous SBA-15 silica) [44].

2.2. scCO_2 as Anti-Solvent

scCO_2 can be used as anti-solvent to precipitate oxide-based materials [45–55]. One way to obtain a precipitate is to expand a scCO_2 -saturated solution of metal (or Si) precursor(s) into a low-pressure environment. First, the solution is brought into contact with scCO_2 , so that the concentration of CO_2 dissolved in the solution is increased and a scCO_2 -saturated solution is obtained. Then, the scCO_2 -saturated solution is allowed to expand into a lower pressure reactor through a nozzle. This rapid depressurisation causes CO_2 to pass to the gaseous state, which involves a transfer of energy from the solution in the form of heat. In this way, super-cooling occurs due to the Joule-Thompson effect. As a result, the precipitation of the target materials is triggered, leading to the formation of nanoparticle morphologies that are not usually accessible by conventional catalyst preparation methods [21].

The other way to obtain a precipitate using scCO_2 as anti-solvent involves the expansion of the metal or silicon precursor(s) solution through a nozzle, directly into the scCO_2 medium (Figure 5) [48]. Under these conditions, the solution and scCO_2 rapidly diffuse into each other and cause the solute to precipitate quickly. It should be noted that the anti-solvent approach does not strictly require scCO_2 but can also be achieved using liquid CO_2 . This kind of controlled precipitation of reactants by dense CO_2 anti-solvent route has been investigated extensively by Hutchings' group to produce metal oxides, including CeO_2 [49–51], Co/Ru-TiO_2 [52], Co_3O_4 [53], and Cu/MnO_x [54,55]. For example, CeO_2 was precipitated from a cerium acetate precursor in methanol solution. scCO_2 was firstly injected into a precipitation vessel, and then the precursor solution was pumped into the precipitation vessel in a co-current mode with scCO_2 . As soon as the droplet and scCO_2 came into contact with each other, the solute precipitated due to the decreased solubility in the scCO_2 -rich medium [49,51]. This route was also used to synthesise SiO_2 -supported metal nanoparticles by spraying a silica sol together with a solution of the metal precursor into the scCO_2 phase [48].

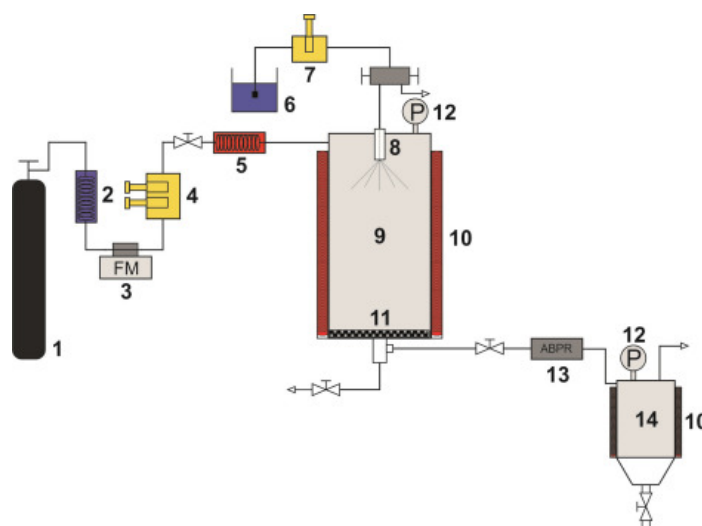


Figure 5. Schematic representation of a set-up for the preparation of oxides using scCO_2 as anti-solvent: (1) CO_2 tank; (2) CO_2 cooler; (3) CO mass flowmeter; (4) CO_2 high-pressure pump; (5) CO_2 pre-heater; (6) precursor solution; (7) high-pressure precursor solution; (8) nozzle; (9) precipitation vessel; (10) heating jacket; (11) metal filter; (12) manometer; (13) automatic back-pressure regulator; (14) separator. (Reprinted with permission from [48]. Copyright Elsevier, 2016).

2.3. Combination of Sol-Gel Methods and $scCO_2$ Drying to Produce Aerogels

The last step of sol-gel syntheses involves the removal of residual solvent (and possibly water) through a drying step. In conventional air-drying processes, pore shrinkage caused by the thermal treatment employed to remove the solvent can result in the collapse of the relatively unstable gel structure. This is due to the large surface tension of the solvent, which implies a strong interaction with the surface of the gel. Consequently, the surface area is undesirably decreased, and the porosity is (partially) lost [56,57]. The solid obtained through such drying process is referred to as a xerogel. Using $scCO_2$ as the drying agent can effectively diminish the degree of structure deformation due to the very low surface tension of $scCO_2$ and the straightforward removal of the carbon dioxide molecules upon depressurisation (which typically occurs at 40–50 °C). The obtained solid is referred to as an aerogel and typically possesses less agglomeration of particles, smaller particle size, higher porosity and higher surface area compared to the corresponding xerogel [56–59]. Sol-gel processes followed by $scCO_2$ drying have been reported extensively for the production of silica [60] and single metal oxide aerogels (such as Al_2O_3 [61], TiO_2 [10], ZrO_2 [62], WO_3 [8], ZnO [5], Cr_2O_3 [6], Fe_2O_3 [63], MoO_3 [64]), doped metal oxide aerogels (such as N- TiO_2 [65], Nb, Ta, and V-doped TiO_2 [66], Ni- Al_2O_3 [67,68]), mixed oxide aerogels (such as TiO_2 - SiO_2 [69], V_2O_5 - TiO_2 [70], ZnO - SnO_2 [71], Al_2O_3 / Sm_2O_3 [72]), as well as nanoparticles supported on oxide aerogels (such as Ag/ Cu - ZrO_2 [73] and Pt/ Co - Al_2O_3 [74]). The process of supercritical drying of gel involves the replacement of molecules entrapped in the pores by either liquid CO_2 or $scCO_2$, and subsequent supercritical drying in a simple batch reactor (as seen in Figure 6). First, the gel can be placed as such in the batch reactor or be immersed in a second solvent (normally an alcohol). The addition of this second solvent is aimed at replacing residual molecules trapped in the gel, in case these are not sufficiently soluble in the (sc) CO_2 phase. Then, (sc) CO_2 is pumped into the reactors until the desired temperature and pressure conditions are reached. Afterwards, the outlet valve of the reactor is opened to allow the solvent to flow out. After all the solvent has been replaced by (sc) CO_2 , the gel can be optionally flushed with (sc) CO_2 for some time. In the last stage, CO_2 is separated from the product by slow depressurisation, leading to isolation of the aerogel.

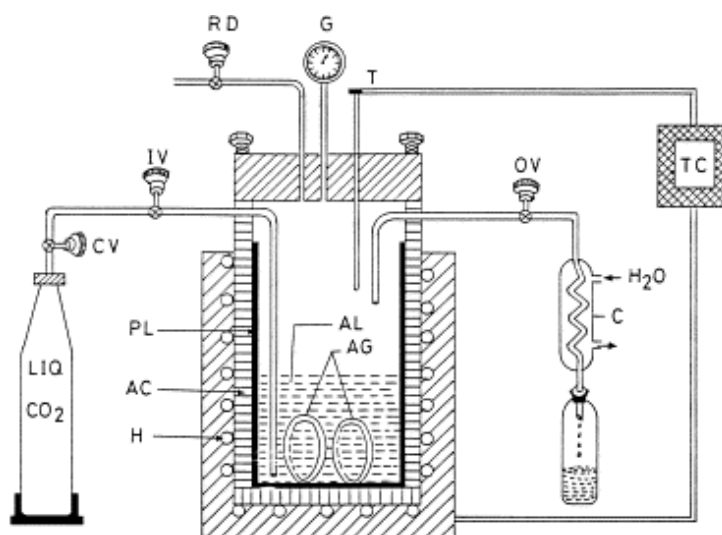


Figure 6. Schematic representation of an equipment for $scCO_2$ drying: H-Heater, AC-autoclave, PL-pyrex liner, CV- CO_2 cylinder valve, IV-inlet valve, OV-outlet valve, C-condenser, RD-rupture disk, G-pressure gauge, T-thermocouple, TC-temperature controller, AL-alcohol (depend on the solvent used for the sol-gel process), AG-aerogel. (Reprinted with permission from [75] Copyright Elsevier, 1999).

3. Catalytic Applications of Nanostructured Oxides Prepared by scCO₂-Assisted Methods

As discussed in the previous sections, nanostructured metal oxides and silicates are a rapidly developing class of materials for catalytic applications, either as supports for metal nanoparticles or as heterogeneous catalysis themselves. In the following sections, a systematic overview is presented of nanostructured oxide-based catalysts prepared by scCO₂-assisted sol-gel methods. The catalysts are grouped by the type of application. First, the specific application of semiconducting metal oxides as photocatalysts is presented in Section 3.1. In photocatalytic processes, the metal oxide enables the use of UV or visible radiation as the energy source to promote a chemical reaction. The following Sections 3.2 and 3.3 provide an overview of oxides with catalytic active sites that are used to promote a chemical reaction without requiring irradiation as energy source. Finally, the use of oxides as supports for metal nanoparticles is presented in Section 3.4. It should be noted that different features of oxides are exploited in each of these applications (though in all cases a large surface area is an asset) and that the same oxide can be used for more than one type of application. In each section, particular attention is dedicated to the relationships between the role of scCO₂ in the synthesis and the physicochemical and catalytic properties of the obtained oxides. Whenever possible, a comparison between the catalytic performance of scCO₂-prepared oxides and that of their counterparts prepared without using scCO₂ is also presented.

3.1. Photocatalysis

Photocatalysts allow the utilisation of electromagnetic radiation as the energy source for conducting a chemical reaction. Typical heterogeneous photocatalysts are semiconductors, i.e., materials that can absorb radiation with a frequency (ν) that corresponds at least to the band gap energy ($h\nu \geq E_{bg}$). The absorption leads to the excitation of an electron to the conduction band, leaving a positive hole in the valence band. These hole-electron pairs allow carrying out redox reactions, including water splitting, the degradation of pollutants in wastewaters, the removal of volatile organic compounds (VOC) and selective oxidation reactions [16]. Several semiconducting metal oxides, such as TiO₂, Fe₂O₃, ZnO, WO₃, SnO₂, NiO, Cu_xO and their composites, have band gaps that allow excitation with UV-Visible radiation and have been reported as photocatalysts (selected examples are reported in Table 2). Among these metal oxides, TiO₂ is commonly regarded as a benchmark heterogeneous photocatalyst, because of its high activity (with UV radiation), thermal and chemical stability, low cost and non-toxicity [76]. TiO₂ has two common crystal structures, the anatase phase with a band gap of 3.23 eV and rutile phase with a band gap of 3.02 eV, corresponding to a threshold in the wavelength of absorbed radiation of 380 and 410 nm, respectively (which implies that TiO₂ mainly absorbs radiation in the UV range and only in a small fraction of the visible range). The anatase phase is generally regarded as the photocatalytically more active phase, but the presence of the rutile phase is considered beneficial for the overall photocatalytic activity. This is attributed to the difference in Fermi levels of anatase and rutile, which implies that the electrons and holes created in one phase can flow into the other phase, thus effectively decreasing the charge recombination and increasing the photocatalytic activity. Degussa P25 TiO₂ is a commercially available TiO₂ catalyst with ~4:1 ratio between anatase and the rutile phase, and is often considered as a reference photocatalyst.

Table 2. Performance in the degradation of pollutants of selected metal-oxide-based photocatalysts prepared by scCO₂-assisted sol-gel methods.

Photocatalyst	Pollutant	Initial Concentration	Radiation Type	T/°C	t/min	Pollutant Removal/Aerogel	Pollutant Removal/Xerogel	Pollutant Removal/P25	Ref.
TiO ₂	Phenol	0.6 mmol/L	UV	25	120	92	4.5	82	[77]
Fe-doped TiO ₂ /WO ₃	Methylene blue	10 ppm	UV	RT ^a	360	77	-	72	[78]
			Visible	RT ^a	720	~67	-	~16	
CdS-ZnS-MPA-TiO ₂	Methylene blue	0.0312 mmol/L	UV	RT ^a	40	88	-	-	[79]
			Visible	RT ^a	240	85	-	-	
40 TiO ₂ -SiO ₂ ^b	Phenol	100 ppm	UV	30	180	51 ^c	-	53 ^d	[42]
	Acetaldehyde	100 ppm	UV	40	40	49 ^c	-	97	
ZnO	Rhodamine B	0.02 mmol/L	UV-Vis	RT ^a	150	100	-	-	[5]
ZnO-SnO ₂	Rhodamine B	0.012 mmol/L	UV	RT ^a	30	100	-	-	[71]

^a Room temperature (exact value not specified).^b The number indicates the loading (wt %) of TiO₂; ^c This catalyst was synthesised by a sol-gel method in scCO₂, and not by scCO₂ drying as the other materials in this table; ^d Amount of P25 comparable with the amount of titania present in 40 TiO₂-SiO₂.

Various methods involving scCO_2 have been developed for the synthesis of TiO_2 . Chen et al. reported an epoxide-assisted sol-gel method to produce a TiO_2 aerogel (Figure 7) [77]. The synthesis involved the hydrolysis and condensation of TiCl_4 with water in the presence of propylene epoxide, followed by scCO_2 drying (40 °C and 80 bar). Propylene oxide has been proposed to act as a gelation agent by neutralising the HCl formed in the hydrolysis of metal chloride precursors [80]. 92% of phenol was degraded by the TiO_2 aerogel (calcined at 650 °C before use) after 120 min UV irradiation at 25 °C, while P25 degraded 82% of phenol and the xerogel produced with the same procedure but with air drying displayed only 4.5% phenol conversion under the same conditions. The higher photocatalytic activity of the aerogel compared to the xerogel was ascribed to the higher surface area of the former (36 vs. 3 m^2/g).

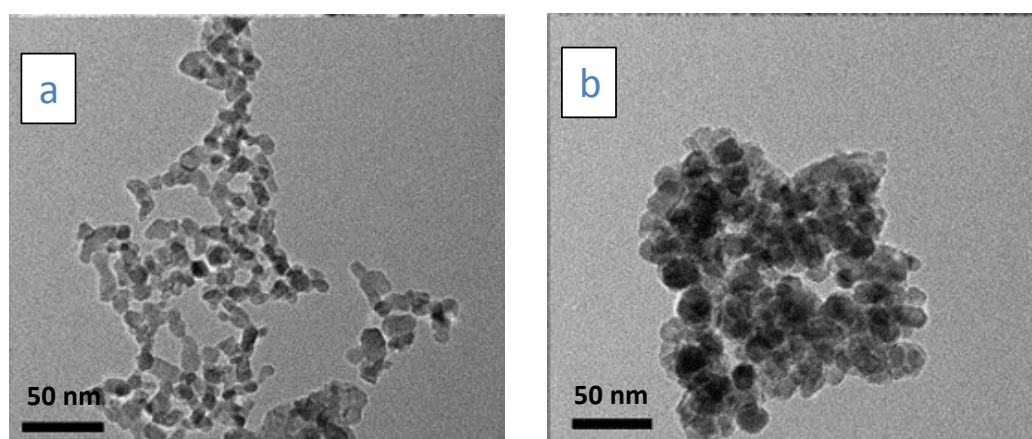


Figure 7. Transmission electron microscopy (TEM) images of aerogel (a) and xerogel (b) TiO_2 samples calcined at 400 °C. (Adapted with permission from [77]. Copyright Elsevier, 2006).

TiO_2 can also be synthesised by a method involving the thermal solvolysis of diisopropoxytitanium bis(acetylacetonate) in scCO_2 [2]. The photocatalytic activity of the obtained TiO_2 was tested in the degradation of methyl orange under UV irradiation. It was found that the synthesis temperature (200–300 °C), and the alcohol used in the solvolysis step (ethanol or isopropanol) affected the surface area and crystallite size, which in turn defined the photocatalytic activity. The TiO_2 prepared under 300 °C and 200 bar scCO_2 afforded the best activity among the prepared materials, and it retained the anatase phase even after calcination to 900 °C. However, comparison with the P25 benchmark was not provided.

A major drawback of TiO_2 as a photocatalyst is that both anatase and rutile absorb mainly radiation in the UV range and thus display low photocatalytic activity with solar light. A strategy to overcome this limitation consists of doping TiO_2 with nonmetals, such as C or N, which endows the material with a visible light response. It has been proposed that carbon or nitrogen doping allows absorption in the visible region by creating intra-band-gap states while not modifying the band gap [81,82]. N-doped TiO_2 aerogel can be obtained by the addition of an ethanolic solution of urea during the hydrolysis of $\text{Ti}(\text{OPr}^i)_4$, followed by scCO_2 drying (40 °C and 101 bar) and/or immersion of the obtained aerogel in an aqueous solution of NH_3 [65]. All the materials displayed the same anatase phase whereas the N-doping led to the expected shift in the absorption towards the visible region (Figure 8). As a consequence, the N-doped TiO_2 aerogels gave a higher photodecomposition of salicylic acid under visible light compared to P25 and a TiO_2 aerogel prepared with the same procedure but without the addition of urea or ammonia.

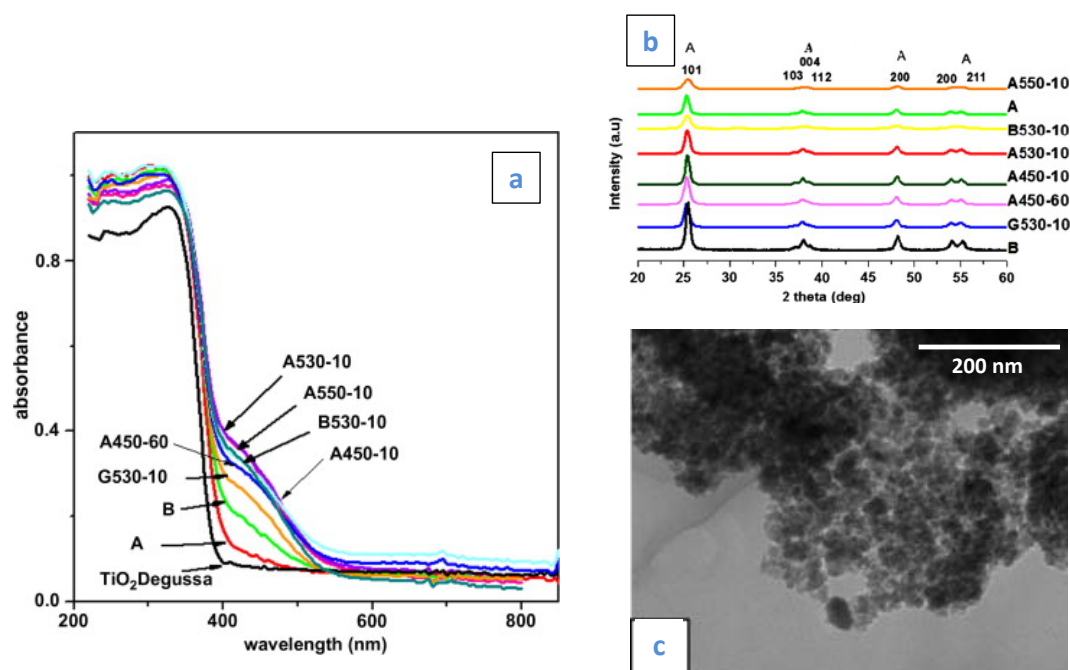


Figure 8. Diffusive reflectance spectra (a) and XRD patterns (b) of the N-doped TiO₂ aerogel and of reference samples; (c) TEM image of the N-doped TiO₂ aerogel A530-10, which gave the highest photocatalytic activity. In the figures, A refers to undoped TiO₂ aerogel, B refers to urea-doped TiO₂ aerogel, G refers to undoped TiO₂ xerogel, whereas the samples immersed in NH₃ are identified by the temperature and time of the thermal treatment that followed the immersion step (e.g., A530-10 is sample A that was thermally treated at 530 °C for 10 min after immersion in NH₃). (Adapted with permission from [65]. Copyright Elsevier, 2010).

The generation of composite semiconductors is another strategy to increase the photocatalytic activity by modifying the band gap and preventing recombination of electrons and holes. Li et al. produced a Fe-doped TiO₂/WO₃ composite aerogel by acid-catalysed hydrolysis of Ti(OBu)₄, WCl₆ and Fe(NO₃)₃, followed by drying with scCO₂ at 42 °C and 110 bar for 8 h. The resulting Fe-doped TiO₂/WO₃ aerogel had a band gap of 2.1 eV and successfully decomposed methylene blue under visible and UV light [78]. Compared to the P25 benchmark catalyst, the aerogel gave higher removal of methylene blue under visible light and similar activity under UV radiation. However, no dark test was performed for evaluating the adsorption capacity of the material.

Charpentier et al. reported the synthesis of a Fe-doped TiO₂/reduced-graphite-oxide composite (Fe-TiO₂/rGO) using a sol-gel method in scCO₂, which acted both as the solvent and drying agent [31]. The sol-gel synthesis method employed FeCl₃ and Ti(OPrⁱ)₄ as metal precursors in a reaction medium containing reduced graphite oxide, isopropanol, acetic acid and scCO₂ (60 °C and 345 bar) in a reactor in which rGO were brought in contact with the reaction mixture only when scCO₂ was present. Afterwards, the formed gel was washed with a continuous scCO₂ flow before calcination. Reduced graphite oxide was used with the aim of lowering the band gap of TiO₂ and to enhance pollutants adsorption. At 0.6% Fe-doping, the band gap significantly decreased from 3.2 to 2.3 eV. The prepared catalysts displayed a higher activity in comparison to both Fe-TiO₂ and TiO₂/rGO composites in the photodegradation of 17β-estradiol under visible light irradiation. However, comparison with the P25 benchmark was not provided. TiO₂ nanowires prepared through the above-mentioned method were also used as a support for CdS-ZnS semiconductor quantum dots (Figure 9), and the obtained material was used as a photocatalyst for the degradation of methylene blue, showing higher photocatalytic activity than P25 [79]. The stability against hydrolysis of the CdS-ZnS quantum dots was not addressed.

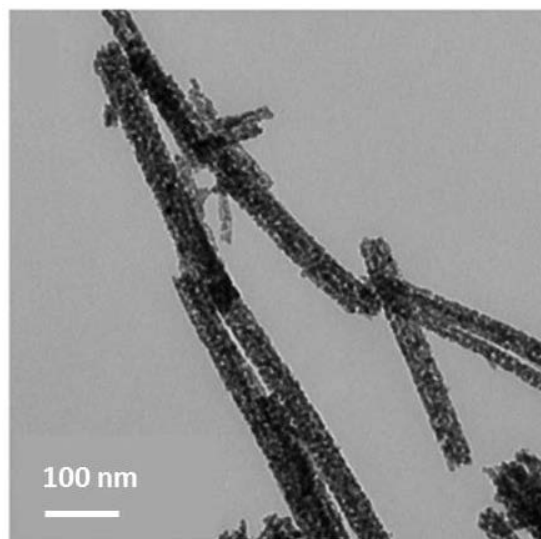


Figure 9. TEM image of CdS-ZnS supported on TiO₂ (Adapted with permission from [79]. Copyright the Royal Society of Chemistry, 2015).

TiO₂/SiO₂ composites with different Ti/Si ratios were synthesised by reacting Si(OMe)₄ and Ti(OPrⁱ)₄ in the presence of formic acid and scCO₂ at 75 °C, with or without a surfactant (Pluronic 17R4) [42]. This non-aqueous synthesis method led to the formation of high surface area composites, reaching the highest value (595 m²/g) for the composite containing 40 wt % TiO₂. This material also displayed the best photocatalytic performance (in terms of TON) in the degradation of phenol in water under UV irradiation within the series of TiO₂/SiO₂ with different TiO₂ wt %. The photocatalyst displayed much higher photocatalytic activity compared to its counterpart prepared in the absence of scCO₂. On the other hand, the performance did not surpass that of P25. This TiO₂/SiO₂ photocatalyst could be reused in consecutive cycles without activity loss and was also active in the gas-phase degradation of acetaldehyde. Yao et al. also prepared TiO₂-SiO₂ composites, though using a different route in which scCO₂ was used as the drying agent. The aerogel possessed high titanium content (up to 50 wt %), well-developed porosity and high surface area (440 m²/g). This TiO₂-SiO₂ aerogel displayed much higher activity in the photocatalytic oxidation of trichloroethylene compared to P25 under the same conditions [69]. However, this study lacked an analysis of the adsorption behaviour of the tested materials, which could play an important role in the observed removal rate of trichloroethylene.

The dispersion of noble metals on the surface of TiO₂ has been investigated with the purpose of enhancing the photocatalytic activity of TiO₂, because metal particles can trap electrons, thus extending the electron-hole pair lifetime [83]. H₂PtCl₆ was impregnated onto the surface of a TiO₂ photocatalyst prepared by supercritical anti-solvent precipitation (see Section 2.2) [84]. The obtained Pt/TiO₂ material calcined at 750 °C was found to have a comparable catalytic performance with Pt/P25 in the water splitting reaction under UV-Vis irradiation. The Pt/TiO₂ displayed a lower surface area (25 vs. 55 m²/g) but a higher anatase content (90 vs. 80%) compared to P25. In another work, Pt nanoparticles were supported on N-TiO₂ aerogel (prepared by a similar method to the above-mentioned N-doped TiO₂ aerogel [65]) by UV photoreduction and tested as photocatalyst for the water splitting reaction [85]. The Pt/N-TiO₂ catalyst reached an H₂ evolution at 7.8 μmol/min under UV-Vis irradiation, about 1.2 times higher than that of a Pt-TiO₂ aerogel prepared with the same method but without N-doping and that of Pt-P25 prepared by replacing N-TiO₂ aerogel with P25 in the synthesis of Pt/N-TiO₂.

Apart from TiO₂-based nanomaterials, ZnO is another common photocatalyst. Krumm et al. reported the preparation of a ZnO aerogel (Figure 10a) with a sol-gel method followed by scCO₂

drying under 50 °C and 60 bar [5]. The obtained material was applied as photocatalyst for the photodegradation of Rhodamine B under UV irradiation and showed higher activity compared to commercial ZnO. The ZnO aerogel was reused three times without activity loss or structural change (Figure 10b). Davis et al. reported the synthesis of a ZnO-SnO₂ aerogel by scCO₂ drying at 40 °C and 76 bar. The obtained photocatalyst was active in the degradation of Rhodamine B under UV irradiation and could be reused in at least three consecutive runs. The activity of the material was attributed to its relatively high surface area (92 m²/g) and to the porous network obtained after scCO₂ drying [71].

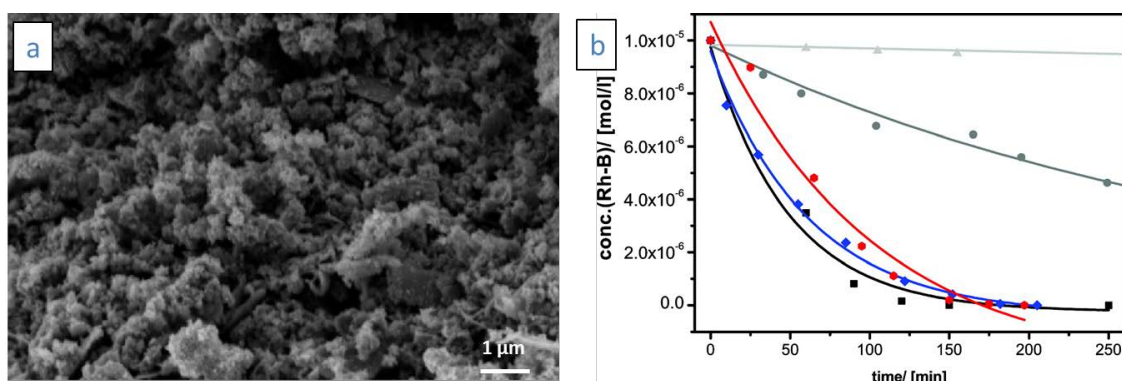


Figure 10. (a) Scanning electron microscopy (SEM) image of the ZnO aerogels obtained by full supercritical drying; (b) photocatalytic degradation of rhodamine B with: ZnO aerogel as the photocatalyst (first cycle: black, second cycle: blue, third cycle: red); commercial ZnO as reference photocatalyst (dark grey); with no photocatalyst (light grey). (Adapted with permission from [5]. Copyright American Chemical Society, 2010).

3.2. Chemocatalytic Oxidation of Organic Compounds

The partial oxidation of hydrocarbon compounds is a class of important chemical reactions of large industrial relevance because the obtained products have a wide range of applications as raw materials or intermediates for the production of polymers, surfactants, and pharmaceuticals. Methane (CH₄) is the simplest hydrocarbon compound and the major component of natural gas. The activation and conversion of CH₄ into higher hydrocarbons would open valuable pathways to produce chemicals which currently are obtained from cracking and refining of crude oil [86]. Neumann et al. reported the oxidative coupling of CH₄ to produce ethane and ethylene along with CO and CO₂ as undesired side products employing Sm₂O₃/Al₂O₃ as the catalyst [72]. The Sm₂O₃/Al₂O₃ material was prepared via a sol-gel process in the presence of an epoxide (the function of the epoxide was discussed in Section 3.1) and ensuing scCO₂ drying. The resulting aerogel was mesoporous and exhibited a higher surface area and pore volume than the air-dried xerogel that underwent structure deformation during solvent removal in air (Figure 11). Moreover, differently from pure Al₂O₃ or Sm₂O₃ aerogels, the Sm₂O₃/Al₂O₃ aerogel retained an amorphous structure even after calcination at 800 °C. The obtained Sm₂O₃/Al₂O₃ catalyst prepared by scCO₂ drying displayed higher CH₄ conversion and C₂ selectivity (and lower CO selectivity) compared to pure Al₂O₃ or Sm₂O₃ catalysts prepared with the same method. This was attributed to an intimate mixing of Al and Sm at the nanoscale. On the other hand, the CH₄ conversion and the C₂ selectivity over the Sm₂O₃/Al₂O₃ aerogel catalyst were lower than those obtained by the Sm₂O₃/Al₂O₃ xerogel or the Sm₂O₃/Al₂O₃ counterpart prepared by the impregnation method, despite the larger surface area of the aerogel.

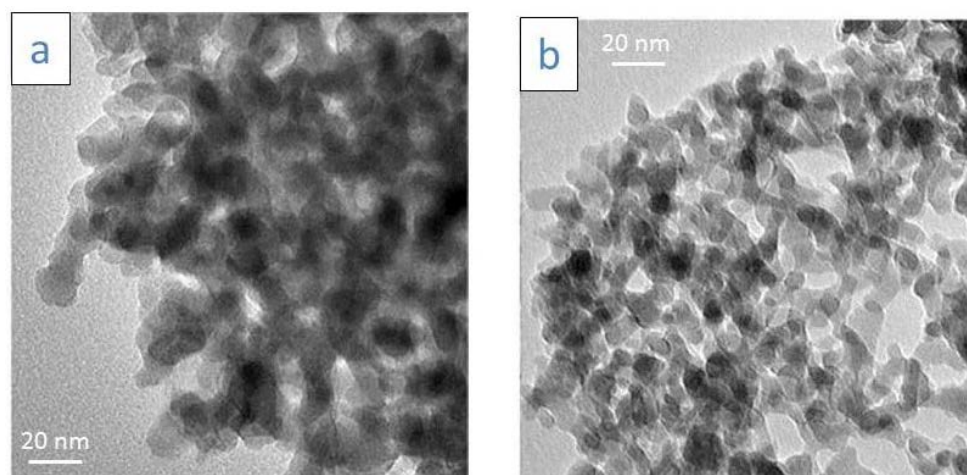


Figure 11. TEM images of $\text{Al}_2\text{O}_3/\text{Sm}_2\text{O}_3$ sol-gel derived materials: (a) xerogel and (b) aerogel calcined in air at $800\text{ }^\circ\text{C}$ for 4 h. (Adapted with permission from [72]. Copyright Springer International Publishing AG, 2015).

Another type of partial oxidation with wide potential for industrial application is the epoxidation of unsaturated hydrocarbons. Ti-containing zeolites (e.g., TS-1, Ti- β) have been studied intensively as catalysts for epoxidation reactions. Ti-containing zeolites are efficient only for oxidation reactions of small substrates due to the small size of their pores (micropores). Moreover, only up to 3 mol % of Ti can be incorporated in the crystalline zeolite framework, which limits the number of active sites of per gram of material. These disadvantages stimulated the development of Ti-Si mixed oxides with higher Ti content and larger pore size as alternative epoxidation catalysts with a much broader substrate scope. Well-known examples of such titanium silicates are the ordered mesoporous materials such as Ti-MCM-41. However, the synthesis of ordered mesoporous silicates requires the use of expensive surfactants acting as structure directing agents. The synthesis of Ti-Si mixed oxides involving scCO_2 drying can represent a simple and low-cost alternative. Müller et al. prepared a series of $\text{TiO}_2\text{-SiO}_2$ [87] and organically modified $\text{TiO}_2\text{-SiO}_2$ aerogels [88] using a sol-gel process combined with low-temperature scCO_2 extraction of propanol used as the solvent ($40\text{ }^\circ\text{C}$ and 230 bar). Trihexylamine (THA) was used to shorten the gelation time. The obtained materials were calcined at $400\text{ }^\circ\text{C}$ prior to their application as catalysts. The 10 wt % $\text{TiO}_2\text{-SiO}_2$ aerogel exhibited a high specific surface area of $813\text{ m}^2/\text{g}$. The amorphous $\text{TiO}_2\text{-SiO}_2$ aerogels were highly active and selective in the epoxidation of cyclohexene and cyclohexanol with *tert*-butyl hydroperoxide (*t*BuOOH) as the oxidant. The same method was also used to prepare organic functionalised $\text{TiO}_2\text{-SiO}_2$ aerogels by including methyltrimethoxysilane (MTES) and phenyltrimethoxysilane (PHTMS) as silicon precursors together with $\text{Si}(\text{OMe})_4$. Compared to the unmodified $\text{TiO}_2\text{-SiO}_2$ aerogel, the phenyl-modified aerogel displayed 2% and 3% increase in cyclohexene and cyclohexenol oxide yields, respectively. The synthesis of $\text{TiO}_2\text{-SiO}_2$ aerogels via supercritical drying was also applied to gels obtained from the pyrolysis of $\text{Ti}[\text{OSi}(\text{O}^t\text{Bu})_3]_4$. The obtained aerogel possessed a high surface area of $667\text{ m}^2/\text{g}$, while the conventional air-dried xerogel displayed a lower surface area of $552\text{ m}^2/\text{g}$. As a consequence, the aerogel $\text{TiO}_2\text{-SiO}_2$ catalyst afforded a higher yield of cyclohexene oxide than the xerogel (49% vs. 36%) in the epoxidation of cyclohexene with *t*BuOOH [89]. Though these $\text{TiO}_2\text{-SiO}_2$ catalysts have wider applicability regarding the size of the substrate compared to Ti-zeolite, it should be noted that they were employed with organic peroxides as oxidants, whereas the green and more affordable H_2O_2 would probably cause leaching of Ti species.

Whereas the partial oxidation of hydrocarbons allows synthesising useful chemical products, the total oxidation of hydrocarbons classified as volatile organic compounds (VOCs) is employed for the elimination of these major atmospheric pollutants, which contribute to the ozone layer depletion

and the greenhouse effect. Marin et al. reported a Co_3O_4 heterogeneous catalyst prepared using supercritical anti-solvent precipitation in CO_2 (Section 2.2) with water as co-solvent and applied it in the total oxidation of propane at 175°C [53]. The use of water in the anti-solvent precipitation process was considered to be crucial since it changed the precipitation environment and promoted the formation of cobalt carbonates instead of cobalt acetate precipitates. The calcination of the metal acetates to form the corresponding oxides results in a decrease in the surface area because the exothermic nature of the decomposition of metal acetates promotes sintering, whereas the endothermic nature of the decomposition of metal carbonates allows better preservation or even leads to an increase in the surface area. As a consequence, after calcination of the solids, the Co_3O_4 catalyst prepared with 10 wt % water demonstrated a higher surface area compared to the catalyst prepared without using water ($32\text{ m}^2/\text{g}$ vs. $16\text{ m}^2/\text{g}$) and a higher propane conversion rate.

Some chlorinated aromatic compounds (e.g., chlorobenzenes) are designated as environmental pollutants and potential precursors for dioxins and polychlorinated dibenzofuran. Choi et al. applied a $\text{V}_2\text{O}_5\text{-TiO}_2$ aerogel as a catalyst for the oxidative degradation of 1,2-dichlorobenzene with O_2 in the temperature range of $150\text{--}160^\circ\text{C}$. Compared to its xerogel counterpart (dried in air) and the impregnated counterpart (ammonium metavanadate solution impregnated on P25), the aerogel catalyst had a higher surface area ($153\text{ m}^2/\text{g}$ vs. $13\text{ m}^2/\text{g}$ and $55\text{ m}^2/\text{g}$ at 5 wt % V_2O_5 loading) and markedly higher catalytic activity (Figure 12). In the synthesis of the aerogel, the titanium precursor was pre-hydrolysed before the addition of the vanadium precursor with the purpose of enhancing the amount of vanadia at the surface of the material. This strategy was followed because surface mono- and poly-vanadates were assumed to be the active species for catalytic oxidation. It was found that the activity was proportional to the loading of vanadium up to 10 wt %. At higher vanadia content, more by-products such as carboxylates, carbonates and phenolates, were formed [70,90].

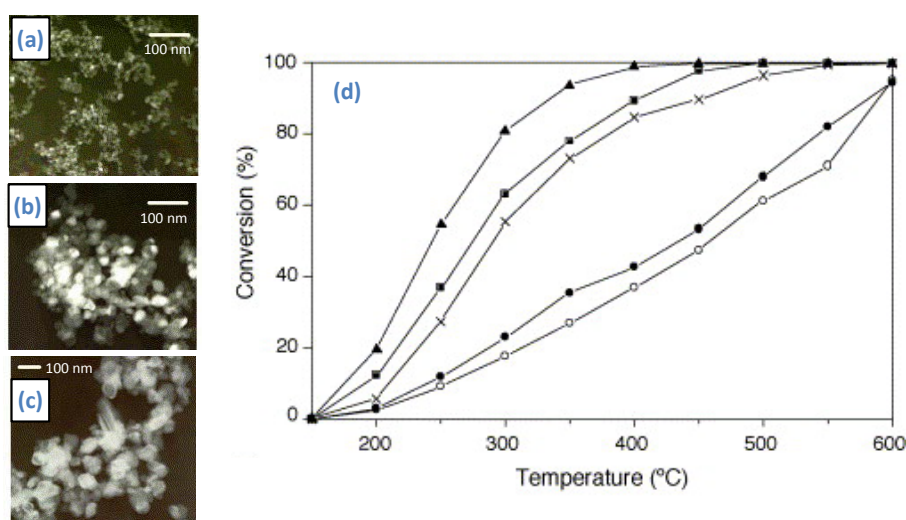


Figure 12. TEM images of: (a) 10 wt % vanadia–titania aerogel; (b) 5 wt % impregnated vanadia–titania; (c) 25 wt % vanadia–titania xerogel; (d) Oxidative degradation of 1,2- dichlorobenzene over the $\text{V}_2\text{O}_5\text{-TiO}_2$ catalysts: 2 wt % vanadia–titania aerogel (●), 5 wt % vanadia–titania aerogel (■), 10 wt % vanadia–titania aerogel (▲), 5 wt % vanadia–titania xerogel (○), 5 wt % impregnated vanadia–titania (×). (Adapted with permission from [70]. Copyright Elsevier, 2006).

3.3. Chemocatalytic Oxidation and Reduction of Inorganic Compounds

The oxidation of inorganic compounds is another class of important chemical reactions. For example, the low-temperature oxidation of CO to CO_2 has attracted attention for application in breathing apparatuses, CO_2 lasers, and space exploration. Among CO oxidation catalysts, the Cu-Mn mixed oxide, known as hopcalite, is a common and affordable catalyst. When preparing this catalyst,

it is of particular importance to avoid the formation of distinct phases containing copper oxide and manganese oxide, which may lead to lower activity in CO oxidation. Hutchings et al. proposed a supercritical anti-solvent precipitation method to prepare high surface area nanostructured oxides with a homogeneous distribution of Cu^{2+} and Mn^{3+} , which were more active in the oxidation of CO at ambient temperature compared to the counterpart catalyst prepared by co-precipitation of copper and manganese nitrate at 80 °C [54]. The addition of water as co-solvent in the supercritical anti-solvent process was found to yield spherical agglomerates of fibrous strings with high surface area because the addition of water promotes the formation of carbonate species from the amorphous acetate precursor (see also the synthesis of Co_3O_4 discussed in Section 3.2 [53]). If the precipitation proceeded in the absence of water, the material displayed a structure consisting of quasi-spherical particles with low surface area [55].

Besides hopcalite, mesoporous Co_3O_4 prepared using a scCO_2 deposition method (Section 2.1) was also applied as a catalyst in low-temperature CO oxidation [44]. In the deposition process, the Co precursor and SBA-15 as hard template were placed separately in the reactor. The deposition only started when the scCO_2 conditions were reached (50 °C, 230 or 130 bar). Then, the impregnated SBA-15 was calcined, and the SBA-15 used as the template was finally removed by base etching. It was found that the CO_2 pressure had a profound effect on the Co_3O_4 morphology: a high CO_2 pressure (230 bar) favoured the formation of an ordered mesoporous structure, while a low CO_2 pressure (130 bar) promoted the formation of randomly organised nanorods. For the Co_3O_4 prepared under 130 bar, CO conversion reached 100% with O_2 as the oxidant at 20 °C.

The conversion of nitrogen oxides (NO , NO_2 and N_2O) and hydrogen sulphide (H_2S) into less harmful compounds has been a subject of considerable interest within green chemistry because these gases can generate acid rain and photochemical smog. Selective catalytic reduction of nitrogen oxides and oxidation of hydrogen sulphide are effective treatments for the elimination of these compounds. The selective catalytic reduction of NO_x with NH_3 and the selective oxidation of H_2S with O_2 were studied over V_2O_5 - TiO_2 aerogel catalysts, which were prepared by a sol-gel method with subsequent drying in supercritical CO_2 . The supercritical-dried V_2O_5 - TiO_2 aerogel catalyst exhibited higher surface area and higher total pore volume compared to the air-dried xerogel counterpart and the impregnated counterpart (V_2O_5 on P25) [91,92]. For both reactions, the V_2O_5 - TiO_2 aerogel displayed better catalytic performance than the xerogel and impregnated counterparts in terms of NO_x conversion [91] and H_2S conversion [92]. The catalytic activity in the NO_x reduction was further optimised by using a V_2O_5 - TiO_2 catalyst prepared by impregnating an ammonium metavanadate aqueous solution on an aerosol TiO_2 . Compared to the above-mentioned V_2O_5 - TiO_2 aerogel prepared by hydrolysis and condensation of vanadium and titanium precursors together, the impregnated V_2O_5 - TiO_2 aerogel achieved higher NO_x conversion in a wider temperature window. This was attributed to a higher fraction of vanadium species being exposed on the surface.

3.4. Nanostructured Oxides as Catalyst Supports

Many heterogeneous catalysts consist of (noble) metal nanoparticles supported on a high surface area material [93–95]. The role of the support is to provide a high dispersion and stabilisation of the nanoparticles to prevent their aggregation and coalescence while granting their accessibility for the catalytic reaction. Additionally, the support should have high chemical and thermal stability and be affordable. Metal oxides and silica can fulfill all these criteria and, therefore, are largely employed as supports. It should be noted that in some cases the support materials contain acid or base sites that may play a catalytic role as well (e.g., Al_2O_3). The nanostructured oxides prepared by scCO_2 -assisted sol-gel processes (such as aerogels) typically possess high surface area and, therefore, have been reported as promising support materials [58,59].

SiO_2 is the most common oxide support for metal nanoparticles. A direct sol-gel method in scCO_2 (as discussed in Section 2.1) was used to produce a macroporous SiO_2 aerogel. Polystyrenes with different hydrophilic groups were used in the sol-gel process as templates to form the ordered

macroporous SiO₂ structure. The composition of the template affected the porosity and surface area (which ranged from 270 to 594 m²/g) of the SiO₂ [9].

γ-Al₂O₃ is another common support material because it possesses mild acidity, high surface area, good chemical and thermal stability (up to 700 °C) and excellent corrosion resistance [93,96]. Charpentier et al. reported a one-pot scCO₂-assisted sol-gel method to prepare different Al₂O₃ materials using Al(OPrⁱ)₃ as the metal precursor and acetic acid as the condensation agent. This process was free of additional water, organic solvents, surfactants, chelating agents or other additives. The synthesis conditions, including the scCO₂ temperature, pressure, concentration and acid/alkoxide ratio, had large effects on the morphology of Al₂O₃ (Figure 13a,b). By optimising the experimental conditions at 80 °C and 414 bar of scCO₂ using Al(OPrⁱ)₃ at a concentration of 0.3 mmol/mL and an acid/alkoxide ratio of 10, alumina nanofibres were formed, with dimensions ranging from 11 to 22 nm in diameter and 500 to 1000 nm in length (Figure 13a) and with surface areas up to 580 m²/g (prior to calcination), which is the highest surface area achieved with this method. The long fibres with high aspect ratio could resist sintering up to 1050 °C [11]. The same group also reported the synthesis of TiO₂ in scCO₂ via a similar route to that used for Al₂O₃, using two different Ti precursors: Ti(OBu)₄ or Ti(OPrⁱ)₄. In line with the findings for Al₂O₃, the morphology of the TiO₂ could be tuned by adjusting the synthesis conditions (Figure 13c,d) [10,97].

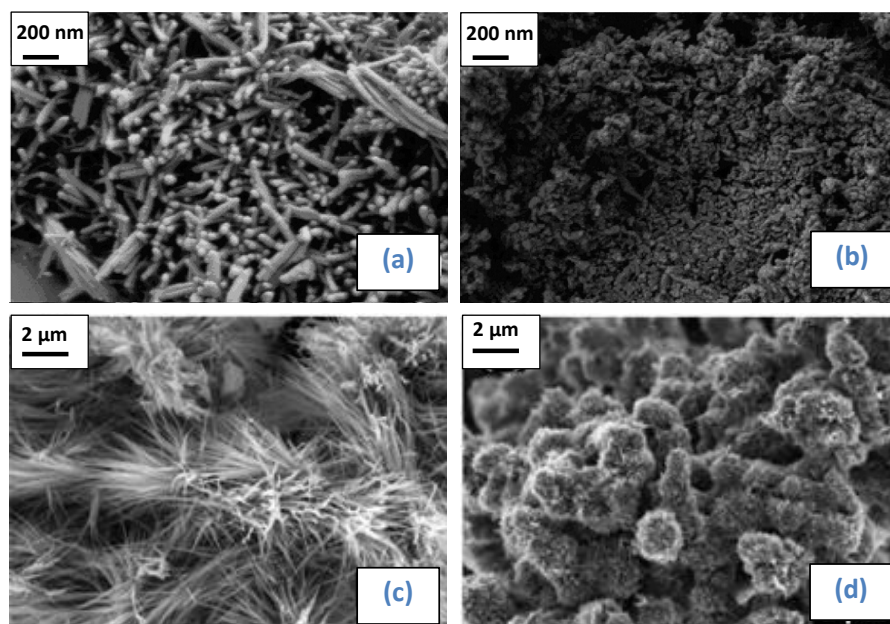


Figure 13. SEM images of alumina particles prepared from aluminium isopropoxide (AIP) and acetic acid in scCO₂ at 80 °C: (a) AIP/scCO₂ = 0.3 mmol/mL, AIP/acetic acid = 1:10, 414 bar; (b) AIP/scCO₂ = 0.5 mmol/mL, AIP/acetic acid = 1:10, 414 bar; (Adapted with permission from [11]. Copyright American Chemical Society, 2009.) and SEM images of titania particles prepared from titanium butoxide (TBO) or titanium isopropoxide (TIP) and acetic acid in scCO₂; (c) 1.1 mol/L TBO, 6.1 mol/L acetic acid, 40 °C, 172 bar; (d) 1.5 mol/L TIP, 6.1 mol/L acetic acid, 60 °C, 414 bar. The samples were measured without grinding or gold coating. (Adapted with permission from [97]. Copyright American Chemical Society, 2005).

Beauger et al. prepared Nb, Ta and V-doped TiO₂ aerogels as supports using scCO₂ drying. The presence of dopants (Nb, Ta or V) helped to preserve the specific surface area of the TiO₂ aerogels during thermal treatment in a reducing atmosphere (32, 44, 45, 59 m²/g for TiO₂, Nb-TiO₂, Ta-TiO₂ and V-TiO₂ with 10 at.% metal doping calcined under 800 °C in H₂/N₂). Doping Nb, Ta and V in TiO₂ influenced the structural, textural and electronic properties of the final material (e.g., surface area, pore volumes, crystallinity, electronic conductivity). For example, Nb or Ta-doped TiO₂ showed

a rutile phase after thermal treatment at 800 °C only in H₂/N₂ while V-TiO₂ could be crystallised to rutile in air [66]. It can be seen from the above examples that the introduction of scCO₂ in the sol-gel synthesis process offers the possibility of achieving high surface area materials and to access specific morphologies. In the following sections, an overview is presented of heterogeneous catalysts in which the oxide support was prepared using scCO₂.

3.4.1. Supported Ni-Based Catalysts

Among transition-metal-based catalysts, oxide-supported Ni catalysts have been widely used in industry due to their relatively low cost and good catalytic activity in (de)hydrogenation reactions.

Reforming Reactions

The utilisation of available resources like natural gas and landfill gas to produce H₂ is of great industrial interests due to a broad range of hydrogen applications including the production of ammonia and methanol, and the hydrogenation of fats and oils. Various reforming technologies have been investigated to generate hydrogen from hydrocarbons or alcohols, including steam reforming, dry (CO₂) reforming and auto-thermal reforming [98]. Ni-based catalysts are commonly employed in reforming processes. However, these catalysts tend to undergo severe deactivation due to carbon deposition on the surface (coking). Synthesising catalysts with smaller and evenly distributed Ni particles on a high-surface-area support has been proposed as an effective strategy to mitigate the coking problem [99]. In this context, a series of Ni-based aerogels were prepared by Song et al. using a sol-gel method followed by scCO₂ drying.

In a first study, a Ni-Al₂O₃ aerogel was synthesised by a sol-gel method and subsequent scCO₂ drying according to the procedure shown in Figure 14 [68]. The aluminium precursor (Al(OBu^s)₃) was pre-hydrolysed with distilled water and nitric acid before the addition of a nickel precursor (nickel acetate). Then, these two precursors underwent hydrolysis and condensation followed by supercritical drying in a scCO₂ stream at 50 °C and 172 bar. For comparison, an impregnated Ni-Al₂O₃ counterpart with the same Ni loading (20 wt %) was prepared by impregnating nickel acetate on an Al₂O₃ aerogel synthesised via the same method mentioned above but without the addition of the nickel precursor. The Ni-Al₂O₃ aerogel exhibited slightly higher surface area (225 vs. 211 m²/g), slightly smaller average particle size, and a higher concentration of active nickel sites on the surface (5.1 vs. 3.9 wt %) compared to the impregnated counterpart. As a consequence, the Ni-Al₂O₃ aerogel exhibited a slightly better catalytic activity in steam reforming of liquefied natural gas. Both catalysts displayed high stability on stream (no decline in activity over 2500 min), whereas commercial Ni-Al₂O₃ deactivated quickly due to coking of the catalyst. The synthesis of Ni-Al₂O₃ aerogel was further investigated by changing Ni/Al ratio [3], by adding propylene oxide as gelation agent (see also Sections 3.1 and 3.2) [100], and by adding La additives [101,102], leading to a slight enhancement in catalytic activity with each approach.

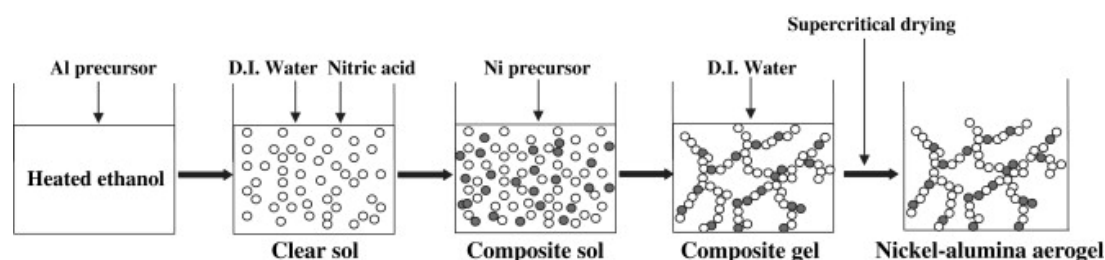


Figure 14. Procedure for the preparation of nickel-alumina aerogel catalyst by a single-step sol-gel method and subsequent supercritical CO₂ drying (Reprinted with permission from [68]. Copyright Elsevier, 2010).

The Ni-Al₂O₃ aerogel (Figure 15a) synthesised with the epoxide-assisted method was also examined as a catalyst in the tri-reforming of methane (combination of steam reforming, partial oxidation, and CO₂ reforming) to produce hydrogen. This reaction has been recognised as the most economical reforming process since it can utilise flue gases (consisting of CH₄, CO₂, and H₂O) without any prior purification. It was found that the catalytic performance of the aerogel was superior to the xerogel counterpart prepared without scCO₂ drying (Figure 15b), and this was attributed to the difference in the surface areas (370 vs. 322 m²/g) and nickel dispersion [103].

The same group extended this epoxide-assisted sol-gel method involving scCO₂ drying to the synthesis of Ni-Al₂O₃-ZrO₂ and Ni-Sr-Al₂O₃-ZrO₂ as catalysts for ethanol reforming to produce H₂ [104,105]. The alkaline-earth metal Sr was used to neutralise the acid sites of Al₂O₃, which can also catalyse the undesired ethanol dehydration reaction. Indeed, higher H₂ yield was obtained with the Sr-containing catalyst. Moreover, this Ni-Sr-Al₂O₃-ZrO₂ aerogel (Figure 15c) displayed higher surface area, larger pore volume and smaller Ni particle size compared to a Ni-Sr-Al₂O₃-ZrO₂ xerogel prepared using a conventional drying method. In addition, the aerogel catalyst demonstrated higher ethanol adsorption capacity as proved by temperature programmed desorption (TPD). All these parameters led to higher H₂ yield with the aerogel catalyst compared to the xerogel counterpart (Figure 15d).

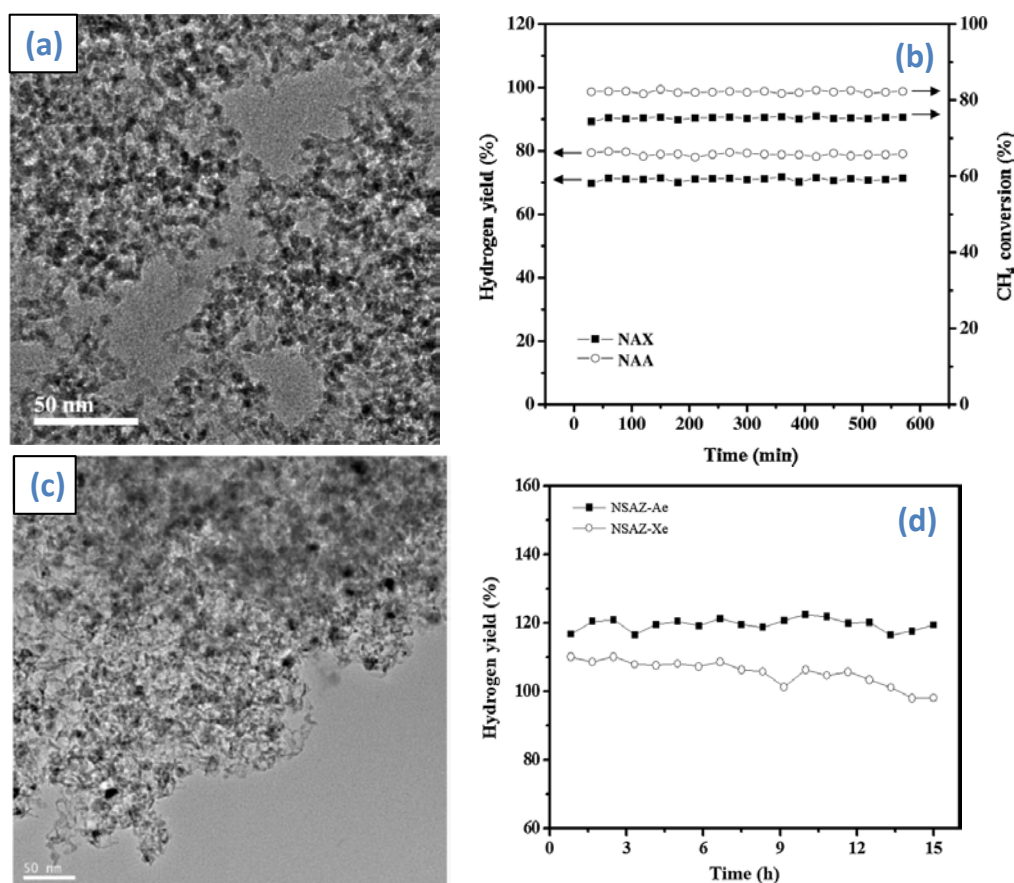


Figure 15. (a) TEM image of Ni-Al₂O₃ aerogel (NAA) catalyst reduced at 700 °C for 3 h; (b) Hydrogen yield and CH₄ conversion with time on stream in the tri-reforming of methane over xerogel Ni-Al₂O₃ (NAX) and NAA catalysts at 700 °C. All the catalysts were reduced at 700 °C for 3 h prior to the reaction. (Adapted with permission from [103]. Copyright Elsevier, 2015); (c) TEM image of Ni-Sr-Al₂O₃-ZrO₂ aerogel (NSAZ-Ae) catalyst reduced at 700 °C for 2 h. (d) Hydrogen yield with time on stream in the steam reforming of ethanol over NSAZ-Ae and Ni-Sr-Al₂O₃-ZrO₂-xerogel (NSAZ-Xe) catalysts at 450 °C. All the catalysts were reduced at 700 °C for 2 h prior to the reaction. (Adapted with permission from [105]. Copyright Elsevier, 2016).

Other Catalytic Reactions

Ni-based aerogel catalysts were also employed in other (de)hydrogenation reactions. Suh et al. prepared Ni-Al₂O₃ and Ni-TiO₂ aerogels by the sol-gel processing of nickel acetate and Al(OBu^s)₃ or Ti(OBu^s)₄ in alcohols and subsequent supercritical drying with CO₂ at 60 °C and 240 bar. The obtained Ni-Al₂O₃ aerogel was applied as the heterogeneous catalyst for the hydrogenation of benzophenone and soybean oil. The catalyst showed much higher conversion rates of benzophenone and soybean oil than those of a catalyst prepared by impregnating the same amount of nickel acetate on commercial Al₂O₃ [67]. The Ni-TiO₂ aerogel was also evaluated in the hydrogenation of benzophenone. It was found that the processing procedure after scCO₂ drying (calcination, reduction) had a large effect on the textual properties (surface area, pore volume) and crystallinity as well as on the catalytic activity in benzophenone conversion of the Ni-TiO₂ aerogels [106]. However, the Ni-TiO₂ showed significantly lower activity compared to the Ni-Al₂O₃ mentioned above: under conditions in which Ni-Al₂O₃ reached 99% conversion in 4 h, the same conversion required 11 h over Ni-TiO₂.

Krompiec et al. used a complexing-agent-assisted sol-gel method combined with scCO₂ drying at 60 °C and 150 bar to produce a Ni-Al₂O₃ aerogel that was used as a heterogeneous catalyst for various (de)hydrogenation reactions. The use of the complexing agent was aimed at controlling the gelation of the aluminium precursor and at obtaining a homogeneous gel of aluminium and nickel species. The role of the complexing agent was to slow down the hydrolysis rate of the aluminium precursor, which is a different approach for matching the hydrolysis rate of the different precursors compared to the use of epoxide as the gelation agent, which should accelerate the hydrolysis rate. The Ni-Al₂O₃ aerogel with large nickel loading (up to 50 wt %) was applied as the catalyst in propene hydrogenation, 1-butene hydrogenation, cyclohexane dehydrogenation, conversion of CO and NO into CO₂ and N₂, CO₂ methanation, and 1-butene isomerisation, though under unchallenging conditions and without comparison to any benchmark [107].

3.4.2. Supported Noble-Metal Nanoparticles Catalysts

Besides the applications in the synthesis of Ni-based materials discussed in the previous section, scCO₂ has also been utilised in the synthesis of oxide-supported noble metal nanoparticles (e.g., Au, Ag, Pd, and Pt). Jespersen et al. reported the synthesis of Pd/SiO₂ by a one-step scCO₂-assisted sol-gel route in which a Pd complex, Si(OMe)₄, polydimethylsiloxane (PDMS) and formic acid underwent sol-gel and drying processes in scCO₂. No organic solvent was involved in this route. The obtained Pd/SiO₂ material was able to catalyse the hydrogenation of 2,5-dihydro-2,5-dimethoxyfuran with a supercritical H₂/CO₂ mixture in both batch (95 °C and 300 bar) and continuous reactors (40 °C and 300 bar), although the performance was not compared to any reference catalyst [40]. A Pt-Co-Al₂O₃ aerogel catalyst was prepared by sol-gel processing of Pt, Co, and Al precursors and subsequent scCO₂ drying. When compared with the counterpart catalyst that was prepared by impregnating chloroplatinic acid and cobalt nitrate on calcined Al₂O₃ aerogel, the aerogel catalyst exhibited a higher catalytic performance for CO oxidation in terms of quicker CO consumption at lower reaction temperature. The enhanced activity for the aerogel catalyst was attributed to the higher surface area and more accessible pores for the reaction substrate of the aerogel catalyst (as proven by N₂-adsorption) [74]. A similar procedure (sol-gel process and ensuing scCO₂ drying) was used to prepare Cu-ZrO₂ and Ag-ZrO₂ aerogels. The catalytic performance of these aerogels in the synthesis of methanol from CO₂ and H₂ was examined. The CO₂ conversion over the Cu-ZrO₂ aerogel was markedly higher than the Cu-ZrO₂ xerogel prepared by co-precipitation, due to the higher copper surface area of the aerogel, as proven by N₂O titration and XPS measurements. Moreover, the Cu-ZrO₂ aerogel was considerably more active than Ag-ZrO₂ in terms of higher CO₂ conversion with similar methanol selectivity [73].

The scCO₂ anti-solvent precipitation technique (see Section 2.2) can also be utilised to prepare oxide supports for nanoparticles. Hutchings et al. applied this method to synthesise CeO₂ support (scCeO₂) for Au [49] and Au-Pd [51] nanoparticles. The nanoparticles were impregnated on the scCeO₂ support by a deposition-precipitation method. Counterpart catalysts were also prepared by

impregnating nanoparticles on the CeO_2 support derived directly from calcination of cerium acetate (unCeO_2). Au-scCeO_2 was used as the catalyst for CO oxidation, and Au-Pd/scCeO_2 was tested in alcohol oxidation. The counterpart catalysts were much less active than the supercritical-precipitated catalysts, which possessed better nanoparticle dispersion. The Au-scCeO_2 and Au-Pd/scCeO_2 catalysts also gave better stability while the Au-Pd/unCeO_2 catalyst suffered gradual deactivation. A similar method was applied to prepare Au-Pd/scTiO_2 catalysts with good nanoparticle dispersion (Figure 16) for the oxidation of benzyl alcohol to benzaldehyde and the synthesis of H_2O_2 [84].

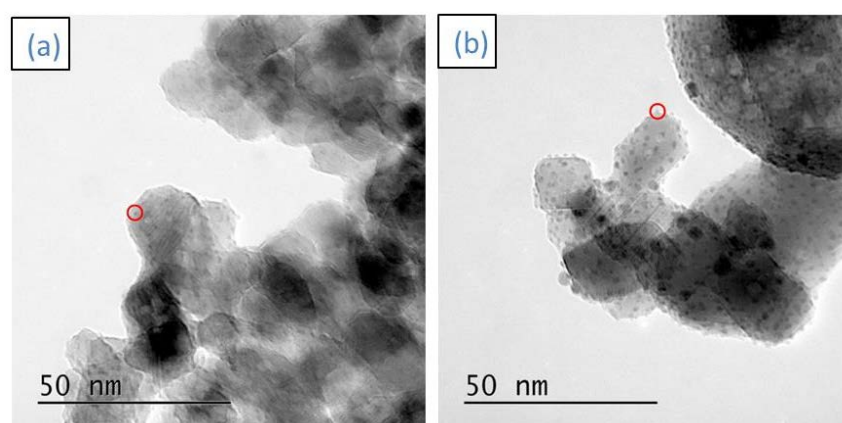


Figure 16. Representative TEM images of 5 wt % AuPd/TiO₂ prepared by supercritical CO₂ anti-solvent method, calcined at (a) 450 °C or (b) 750 °C. The areas circled in red highlight a metal nanoparticle (Adapted with permission from [84]. Copyright Elsevier, 2015).

4. Conclusions and Perspectives

In this review, the recent progress in the field of the synthesis of nanostructured metal oxides, silicates and oxide-supported nanoparticles using scCO_2 -assisted synthesis methods was presented and discussed. These nanomaterials were applied as catalysts for various applications ranging from photocatalysis to oxidation, reduction, and isomerisation reactions. Most of these materials displayed enhanced physicochemical properties (e.g., surface area, porous structure, pore volume and acidity) owing to the scCO_2 -assisted method of synthesis, typically leading to improved catalytic performance. Many of the catalysts presented in this review demonstrate that scCO_2 drying is an established and reliable method to improve the performance of catalytic materials. Future work will possibly expand this approach to the synthesis of metal oxide and silicate aerogels with yet unexplored compositions. On the other hand, the solvent and anti-solvent role of scCO_2 have been less extensively studied and still offer opportunities for new developments by creative design of the reactor set-up. Moreover, these approaches are promising for preparing mixed oxide catalysts in which the different metals (and Si) are homogeneously distributed rather than forming domains of the separate monometallic oxides. Following these or other novel routes, it is expected that future research will expand the potential of scCO_2 -assisted sol-gel routes for the synthesis of new nanostructured metal oxides and silicates for catalytic applications. Further advances are expected through a deeper understanding of the mechanisms of the scCO_2 -assisted syntheses of nanostructured oxides using in situ techniques. Given the possible industrial applications, the up-scaling of scCO_2 -assisted synthesis methods for the production of oxide catalysts should also be addressed.

Acknowledgments: Yehan Tao acknowledges financial support from the China Scholarship Council (CSC) for her Ph.D. grant.

Conflicts of Interest: The authors declare no conflict of interest.

References

1. Patzke, G.R.; Zhou, Y.; Kontic, R.; Conrad, F. Oxide nanomaterials: Synthetic developments, mechanistic studies, and technological innovations. *Angew. Chem. Int. Ed.* **2011**, *50*, 826–859. [[CrossRef](#)] [[PubMed](#)]
2. Alonso, E.; Montequi, I.; Cocero, M. Effect of synthesis conditions on photocatalytic activity of TiO₂ powders synthesized in supercritical CO₂. *J. Supercrit. Fluids* **2009**, *49*, 233–238. [[CrossRef](#)]
3. Seo, J.G.; Youn, M.H.; Bang, Y.; Song, I.K. Effect of Ni/Al atomic ratio of mesoporous Ni-Al₂O₃ aerogel catalysts on their catalytic activity for hydrogen production by steam reforming of liquefied natural gas (LNG). *Int. J. Hydrogen Energy* **2010**, *35*, 12174–12181. [[CrossRef](#)]
4. Lan, Y.; Li, X.; Li, G.; Luo, Y. Sol-gel method to prepare graphene/Fe₂O₃ aerogel and its catalytic application for the thermal decomposition of ammonium perchlorate. *J. Nanopart. Res.* **2015**, *17*, 395. [[CrossRef](#)]
5. Krumm, M.; Pueyo, C.L.; Polarz, S. Monolithic zinc oxide aerogels from organometallic sol-gel precursors. *Chem. Mater.* **2010**, *22*, 5129–5136. [[CrossRef](#)]
6. Gash, A.E.; Tillotson, T.M.; Satcher, J.H., Jr.; Hrubesh, L.W.; Simpson, R.L. New sol-gel synthetic route to transition and main-group metal oxide aerogels using inorganic salt precursors. *J. Non-Cryst. Solids* **2001**, *285*, 22–28. [[CrossRef](#)]
7. Zeng, T.; Zhang, X.; Wang, S.; Niu, H.; Cai, Y. Spatial confinement of a Co₃O₄ catalyst in hollow metal-organic frameworks as a nanoreactor for improved degradation of organic pollutants. *Environ. Sci. Technol.* **2015**, *49*, 2350–2357. [[CrossRef](#)] [[PubMed](#)]
8. Novak, Z.; Kotnik, P.; Knez, Ž. Preparation of WO₃ aerogel catalysts using supercritical CO₂ drying. *J. Non-Cryst. Solids* **2004**, *350*, 308–313. [[CrossRef](#)]
9. Cabañas, A.; Enciso, E.; Carbajo, M.C.; Torralvo, M.J.; Pando, C.; Renuncio, J.A.R. Synthesis of SiO₂-aerogel inverse opals in supercritical carbon dioxide. *Chem. Mater.* **2005**, *17*, 6137–6145. [[CrossRef](#)]
10. Sui, R.; Rizkalla, A.; Charpentier, P.A. Experimental study on the morphology and porosity of TiO₂ aerogels synthesized in supercritical carbon dioxide. *Microporous Mesoporous Mater.* **2011**, *142*, 688–695. [[CrossRef](#)]
11. Chowdhury, M.B.; Sui, R.; Lucky, R.A.; Charpentier, P.A. One-pot procedure to synthesize high surface area alumina nanofibers using supercritical carbon dioxide. *Langmuir* **2009**, *26*, 2707–2713. [[CrossRef](#)] [[PubMed](#)]
12. Gleiter, H. Nanostructured materials: Basic concepts and microstructure. *Acta Mater.* **2000**, *48*, 1–29. [[CrossRef](#)]
13. Bhattacharyya, S.; Lelong, G.; Saboungi, M.-L. Recent progress in the synthesis and selected applications of MCM-41: A short review. *J. Exp. Nanosci.* **2006**, *1*, 375–395. [[CrossRef](#)]
14. Sui, R.; Charpentier, P. Synthesis of metal oxide nanostructures by direct sol-gel chemistry in supercritical fluids. *Chem. Rev.* **2012**, *112*, 3057–3082. [[CrossRef](#)] [[PubMed](#)]
15. Frenzer, G.; Maier, W.F. Amorphous porous mixed oxides: Sol-gel ways to a highly versatile class of materials and catalysts. *Annu. Rev. Mater. Res.* **2006**, *36*, 281–331. [[CrossRef](#)]
16. Tseng, T.K.; Lin, Y.S.; Chen, Y.J.; Chu, H. A review of photocatalysts prepared by sol-gel method for VOCs removal. *Int. J. Mol. Sci.* **2010**, *11*, 2336–2361. [[CrossRef](#)] [[PubMed](#)]
17. Debecker, D.P.; Mutin, P.H. Non-hydrolytic sol-gel routes to heterogeneous catalysts. *Chem. Soc. Rev.* **2012**, *41*, 3624–3650. [[CrossRef](#)] [[PubMed](#)]
18. Debecker, D.P.; Hulea, V.; Mutin, P.H. Mesoporous mixed oxide catalysts via non-hydrolytic sol-gel: A review. *Appl. Catal. A* **2013**, *451*, 192–206. [[CrossRef](#)]
19. Seisenbaeva, G.A.; Kessler, V.G. Precursor directed synthesis—“molecular” mechanisms in the Soft Chemistry approaches and their use for template-free synthesis of metal, metal oxide and metal chalcogenide nanoparticles and nanostructures. *Nanoscale* **2014**, *6*, 6229–6244. [[CrossRef](#)] [[PubMed](#)]
20. Kessler, V.G.; Spijksma, G.I.; Seisenbaeva, G.A.; Håkansson, S.; Blank, D.H.; Bouwmeester, H.J. New insight in the role of modifying ligands in the sol-gel processing of metal alkoxide precursors: A possibility to approach new classes of materials. *J. Sol-Gel Sci. Technol.* **2006**, *40*, 163–179. [[CrossRef](#)]
21. Sanli, D.; Bozbag, S.; Erkey, C. Synthesis of nanostructured materials using supercritical CO₂: Part I. Physical transformations. *J. Mater. Sci.* **2012**, *47*, 2995–3025. [[CrossRef](#)]
22. Bozbag, S.; Sanli, D.; Erkey, C. Synthesis of nanostructured materials using supercritical CO₂: Part II. Chemical transformations. *J. Mater. Sci.* **2012**, *47*, 3469–3492. [[CrossRef](#)]
23. Zhang, X.; Heinonen, S.; Levänen, E. Applications of supercritical carbon dioxide in materials processing and synthesis. *RSC Adv.* **2014**, *4*, 61137–61152. [[CrossRef](#)]

24. Duan, H.; Wang, D.; Li, Y. Green chemistry for nanoparticle synthesis. *Chem. Soc. Rev.* **2015**, *44*, 5778–5792. [[CrossRef](#)] [[PubMed](#)]
25. Cansell, F.; Aymonier, C. Design of functional nanostructured materials using supercritical fluids. *J. Supercrit. Fluids* **2009**, *47*, 508–516. [[CrossRef](#)]
26. Marre, S.; Jensen, K.F. Synthesis of micro and nanostructures in microfluidic systems. *Chem. Soc. Rev.* **2010**, *39*, 1183–1202. [[CrossRef](#)] [[PubMed](#)]
27. Ramsey, E.; Qiubai, S.; Zhang, Z.; Zhang, C.; Wei, G. Mini-Review: Green sustainable processes using supercritical fluid carbon dioxide. *J. Environ. Sci.* **2009**, *21*, 720–726. [[CrossRef](#)]
28. Loy, D.A.; Russick, E.M.; Yamanaka, S.A.; Baugher, B.M.; Shea, K.J. Direct formation of aerogels by sol-gel polymerizations of alkoxy silanes in supercritical carbon dioxide. *Chem. Mater.* **1997**, *9*, 2264–2268. [[CrossRef](#)]
29. Sui, R.; Rizkalla, A.S.; Charpentier, P.A. Kinetics study on the sol-gel reactions in supercritical CO₂ by using in situ ATR-FTIR spectrometry. *Cryst. Growth Des.* **2008**, *8*, 3024–3031. [[CrossRef](#)]
30. Sui, R.; Rizkalla, A.S.; Charpentier, P.A. Synthesis and formation of silica aerogel particles by a novel sol-gel route in supercritical carbon dioxide. *J. Phys. Chem. B* **2004**, *108*, 11886–11892. [[CrossRef](#)]
31. Farhangi, N.; Chowdhury, R.R.; Medina-Gonzalez, Y.; Ray, M.B.; Charpentier, P.A. Visible light active Fe doped TiO₂ nanowires grown on graphene using supercritical CO₂. *Appl. Catal. B* **2011**, *110*, 25–32. [[CrossRef](#)]
32. Lucky, R.A.; Charpentier, P.A. N-doped ZrO₂/TiO₂ bimetallic materials synthesized in supercritical CO₂: Morphology and photocatalytic activity. *Appl. Catal. B* **2010**, *96*, 516–523. [[CrossRef](#)]
33. Lucky, R.A.; Medina-Gonzalez, Y.; Charpentier, P.A. Zr doping on one-dimensional titania nanomaterials synthesized in supercritical carbon dioxide. *Langmuir* **2010**, *26*, 19014–19021. [[CrossRef](#)] [[PubMed](#)]
34. Lucky, R.A.; Charpentier, P.A. A One-step approach to the synthesis of ZrO₂-modified TiO₂ nanotubes in supercritical carbon dioxide. *Adv. Mater.* **2008**, *20*, 1755–1759. [[CrossRef](#)]
35. Lucky, R.; Charpentier, P. A thermal study on the structural changes of bimetallic ZrO₂-modified TiO₂ nanotubes synthesized using supercritical CO₂. *Nanotechnology* **2009**, *20*, 195601. [[CrossRef](#)] [[PubMed](#)]
36. Charpentier, P.A.; Li, X.; Sui, R. Study of the sol-gel reaction mechanism in supercritical CO₂ for the formation of SiO₂ nanocomposites. *Langmuir* **2009**, *25*, 3748–3754. [[CrossRef](#)] [[PubMed](#)]
37. Salarian, M.; Xu, W.Z.; Wang, Z.; Sham, T.-K.; Charpentier, P.A. Hydroxyapatite-TiO₂-based nanocomposites synthesized in supercritical CO₂ for bone tissue engineering: Physical and mechanical properties. *ACS Appl. Mater. Interfaces* **2014**, *6*, 16918–16931. [[CrossRef](#)] [[PubMed](#)]
38. Jensen, H.; Bremholm, M.; Nielsen, R.P.; Joensen, K.D.; Pedersen, J.S.; Birkedal, H.; Chen, Y.S.; Almer, J.; Søgaard, E.G.; Iversen, S.B. In situ high-energy synchrotron radiation study of sol-gel nanoparticle formation in supercritical fluids. *Angew. Chem. Int. Ed.* **2007**, *46*, 1113–1116. [[CrossRef](#)] [[PubMed](#)]
39. Durand, V.; Drobek, M.; Duchateau, M.; Hertz, A.; Ruiz, J.-C.; Sarrade, S.; Guizard, C.; Julbe, A. Potential of sub- and supercritical CO₂ reaction media for sol-gel deposition of silica-based molecular sieve membranes. *Sep. Purif. Technol.* **2014**, *121*, 30–37. [[CrossRef](#)]
40. Jespersen, H.T.; Štandeker, S.; Novak, Z.; Schaumburg, K.; Madsen, J.; Knez, Ž. Supercritical fluids applied to the sol-gel process for preparation of AEROMOSILS/palladium particle nanocomposite catalyst. *J. Supercrit. Fluids* **2008**, *46*, 178–184. [[CrossRef](#)]
41. Hertz, A.; Corre, Y.-M.; Sarrade, S.; Guizard, C.; Julbe, A.; Ruiz, J.-C.; Fournel, B. Ytria stabilized zirconia synthesis in supercritical CO₂: Understanding of particle formation mechanisms in CO₂/co-solvent systems. *J. Eur. Ceram. Soc.* **2010**, *30*, 1691–1698. [[CrossRef](#)]
42. Jammaer, J.; Aprile, C.; Verbruggen, S.W.; Lenaerts, S.; Pescarmona, P.P.; Martens, J.A. A non-aqueous synthesis of TiO₂/SiO₂ composites in supercritical CO₂ for the photodegradation of pollutants. *ChemSusChem* **2011**, *4*, 1457–1463. [[CrossRef](#)] [[PubMed](#)]
43. Jiao, J.; Xu, Q.; Li, L. Porous TiO₂/SiO₂ composite prepared using PEG as template direction reagent with assistance of supercritical CO₂. *J. Colloid Interface Sci.* **2007**, *316*, 596–603. [[CrossRef](#)] [[PubMed](#)]
44. Zhang, Y.; Wang, A.; Huang, Y.; Xu, Q.; Yin, J.; Zhang, T. Nanocasting synthesis of mesostructured Co₃O₄ via a supercritical CO₂ deposition method and the catalytic performance for CO oxidation. *Catal. Lett.* **2012**, *142*, 275–281. [[CrossRef](#)]
45. Jiang, H.; Huang, P.; Liu, L.; Zhang, M. Controllable synthesis of Ce_{1-x}Zr_xO₂ hollow nanospheres via supercritical anti-solvent precipitation. *Mater. Charact.* **2012**, *63*, 98–104. [[CrossRef](#)]

46. Wang, H.; Jiang, H.; Kuang, L.; Zhang, M. Synthesis of highly dispersed $\text{MnO}_x\text{-CeO}_2$ nanospheres by surfactant-assisted supercritical anti-solvent (SAS) technique: The important role of the surfactant. *J. Supercrit. Fluids* **2014**, *92*, 84–92. [[CrossRef](#)]
47. Jiang, H.; Wang, H.; Kuang, L.; Li, G.; Zhang, M. Synthesis of $\text{MnO}_x\text{-CeO}_2\cdot\text{NO}_x$ catalysts by polyvinylpyrrolidone-assisted supercritical antisolvent precipitation. *J. Mater. Res.* **2014**, *29*, 2188–2197. [[CrossRef](#)]
48. Nesterov, N.; Paharukova, V.; Yakovlev, V.; Martyanov, O. The facile synthesis of Ni-Cu catalysts stabilized in SiO_2 framework via a supercritical antisolvent approach. *J. Supercrit. Fluids* **2016**, *112*, 119–127. [[CrossRef](#)]
49. Tang, Z.-R.; Edwards, J.K.; Bartley, J.K.; Taylor, S.H.; Carley, A.F.; Herzing, A.A.; Kiely, C.J.; Hutchings, G.J. Nanocrystalline cerium oxide produced by supercritical antisolvent precipitation as a support for high-activity gold catalysts. *J. Catal.* **2007**, *249*, 208–219. [[CrossRef](#)]
50. Hutchings, G.J. Catalyst synthesis using supercritical carbon dioxide: A green route to high activity materials. *Top. Catal.* **2009**, *52*, 982–987. [[CrossRef](#)]
51. Miedziak, P.J.; Tang, Z.; Davies, T.E.; Enache, D.I.; Bartley, J.K.; Carley, A.F.; Herzing, A.A.; Kiely, C.J.; Taylor, S.H.; Hutchings, G.J. Ceria prepared using supercritical antisolvent precipitation: A green support for gold-palladium nanoparticles for the selective catalytic oxidation of alcohols. *J. Mater. Chem.* **2009**, *19*, 8619–8627. [[CrossRef](#)]
52. Marin, R.P.; Kondrat, S.A.; Gallagher, J.R.; Enache, D.I.; Smith, P.; Boldrin, P.; Davies, T.E.; Bartley, J.K.; Combes, G.B.; Williams, P.B. Preparation of Fischer-Tropsch supported cobalt catalysts using a new gas anti-solvent process. *ACS Catal.* **2013**, *3*, 764–772. [[CrossRef](#)]
53. Marin, R.P.; Kondrat, S.A.; Pinnell, R.K.; Davies, T.E.; Golunski, S.; Bartley, J.K.; Hutchings, G.J.; Taylor, S.H. Green preparation of transition metal oxide catalysts using supercritical CO_2 anti-solvent precipitation for the total oxidation of propane. *Appl. Catal. B* **2013**, *140*, 671–679. [[CrossRef](#)]
54. Tang, Z.-R.; Jones, C.D.; Aldridge, J.K.; Davies, T.E.; Bartley, J.K.; Carley, A.F.; Taylor, S.H.; Allix, M.; Dickinson, C.; Rosseinsky, M.J. New nanocrystalline Cu/ MnO_x catalysts prepared from supercritical antisolvent precipitation. *ChemCatChem* **2009**, *1*, 247–251. [[CrossRef](#)]
55. Tang, Z.-R.; Kondrat, S.A.; Dickinson, C.; Bartley, J.K.; Carley, A.F.; Taylor, S.H.; Davies, T.E.; Allix, M.; Rosseinsky, M.; Claridge, J. Synthesis of high surface area CuMn_2O_4 by supercritical anti-solvent precipitation for the oxidation of CO at ambient temperature. *Catal. Sci. Technol.* **2011**, *1*, 740–746. [[CrossRef](#)]
56. Choi, J.; Suh, D.J. Catalytic applications of aerogels. *Catal. Surv. Asia* **2007**, *11*, 123–133. [[CrossRef](#)]
57. Pierre, A.C.; Pajonk, G.M. Chemistry of aerogels and their applications. *Chem. Rev.* **2002**, *102*, 4243–4266. [[CrossRef](#)] [[PubMed](#)]
58. Pajonk, G. Aerogel catalysts. *Appl. Catal.* **1991**, *72*, 217–266. [[CrossRef](#)]
59. Pajonk, G. Catalytic aerogels. *Catal. Today* **1997**, *35*, 319–337. [[CrossRef](#)]
60. Dorcheh, A.S.; Abbasi, M. Silica aerogel; synthesis, properties and characterization. *J. Mater. Process. Technol.* **2008**, *199*, 10–26. [[CrossRef](#)]
61. Poco, J.; Satcher, J.; Hrubesh, L. Synthesis of high porosity, monolithic alumina aerogels. *J. Non-Cryst. Solids* **2001**, *285*, 57–63. [[CrossRef](#)]
62. Sui, R.; Rizkalla, A.S.; Charpentier, P.A. Direct synthesis of zirconia aerogel nanoarchitecture in supercritical CO_2 . *Langmuir* **2006**, *22*, 4390–4396. [[CrossRef](#)] [[PubMed](#)]
63. Gash, A.E.; Tillotson, T.M.; Satcher, J.H., Jr.; Poco, J.F.; Hrubesh, L.W.; Simpson, R.L. Use of epoxides in the sol-gel synthesis of porous iron (III) oxide monoliths from Fe (III) salts. *Chem. Mater.* **2001**, *13*, 999–1007. [[CrossRef](#)]
64. Dong, W.; Mansour, A.; Dunn, B. Structural and electrochemical properties of amorphous and crystalline molybdenum oxide aerogels. *Solid State Ionics* **2001**, *144*, 31–40. [[CrossRef](#)]
65. Popa, M.; Macovei, D.; Indrea, E.; Mercioniu, I.; Popescu, I.; Danciu, V. Synthesis and structural characteristics of nitrogen doped TiO_2 aerogels. *Microporous Mesoporous Mater.* **2010**, *132*, 80–86. [[CrossRef](#)]
66. Beauger, C.; Testut, L.; Berthon-Fabry, S.; Georgi, F.; Guétaz, L. Doped TiO_2 aerogels as alternative catalyst supports for proton exchange membrane fuel cells: A comparative study of Nb, V and Ta dopants. *Microporous Mesoporous Mater.* **2016**, *232*, 109–118. [[CrossRef](#)]
67. Suh, D.J.; Park, T.-J.; Lee, S.-H.; Kim, K.-L. Nickel-alumina composite aerogels as liquid-phase hydrogenation catalysts. *J. Non-Cryst. Solids* **2001**, *285*, 309–316. [[CrossRef](#)]

68. Seo, J.G.; Youn, M.H.; Jung, J.C.; Song, I.K. Hydrogen production by steam reforming of liquefied natural gas (LNG) over mesoporous nickel-alumina aerogel catalyst. *Int. J. Hydrogen Energy* **2010**, *35*, 6738–6746. [[CrossRef](#)]
69. Yao, N.; Cao, S.; Yeong, K.L. Mesoporous TiO₂-SiO₂ aerogel with hierarchal pore structures. *Microporous Mesoporous Mater.* **2009**, *117*, 570–579. [[CrossRef](#)]
70. Choi, J.; Shin, C.B.; Park, T.-J.; Suh, D.J. Characteristics of vanadia-titania aerogel catalysts for oxidative destruction of 1, 2-dichlorobenzene. *Appl. Catal. A* **2006**, *311*, 105–111. [[CrossRef](#)]
71. Davis, M.; Hikal, W.M.; Gümeçi, C.; Hope-Weeks, L.J. Aerogel nanocomposites of ZnO-SnO₂ as efficient photocatalysts for the degradation of Rhodamine B. *Catal. Sci. Technol.* **2012**, *2*, 922–924. [[CrossRef](#)]
72. Neumann, B.; Elkins, T.W.; Gash, A.E.; Hagelin-Weaver, H.; Bäumer, M. Sol-gel preparation of samaria catalysts for the oxidative coupling of methane. *Catal. Lett.* **2015**, *145*, 1251–1261. [[CrossRef](#)]
73. Köppel, R.A.; Stöcker, C.; Baiker, A. Copper-and silver-zirconia aerogels: Preparation, structural properties and catalytic behavior in methanol synthesis from carbon dioxide. *J. Catal.* **1998**, *179*, 515–527. [[CrossRef](#)]
74. Kwak, C.; Park, T.-J.; Suh, D.J. Preferential oxidation of carbon monoxide in hydrogen-rich gas over platinum-cobalt-alumina aerogel catalysts. *Chem. Eng. Sci.* **2005**, *60*, 1211–1217. [[CrossRef](#)]
75. Wagh, P.B.; Begag, R.; Pajonk, G.M.; Venkateswara Rao, A.; Haranath, D. Comparison of some physical properties of silica aerogel monoliths synthesized by different precursors. *Mater. Chem. Phys.* **1999**, *57*, 214–218.
76. Guo, G.; Whitesell, J.K.; Fox, M.A. Synthesis of TiO₂ photocatalysts in supercritical CO₂ via a non-hydrolytic route. *J. Phys. Chem. B* **2005**, *109*, 18781–18785. [[CrossRef](#)] [[PubMed](#)]
77. Chen, L.; Zhu, J.; Liu, Y.-M.; Cao, Y.; Li, H.-X.; He, H.-Y.; Dai, W.-L.; Fan, K.-N. Photocatalytic activity of epoxide sol-gel derived titania transformed into nanocrystalline aerogel powders by supercritical drying. *J. Mol. Catal. A Chem.* **2006**, *255*, 260–268. [[CrossRef](#)]
78. Li, H.; Sunol, S.; Sunol, A. Development of titanium-dioxide-based aerogel catalyst with tunable nanoporosity and photocatalytic activity. *Nanotechnology* **2012**, *23*, 294012. [[CrossRef](#)] [[PubMed](#)]
79. Mumin, M.A.; Moula, G.; Charpentier, P.A. Supercritical CO₂ synthesized TiO₂ nanowires covalently linked with core-shell CdS-ZnS quantum dots: Enhanced photocatalysis and stability. *RSC Adv.* **2015**, *5*, 67767–67779. [[CrossRef](#)]
80. Tillotson, T.; Sunderland, W.; Thomas, I.; Hrubesh, L. Synthesis of lanthanide and lanthanide-silicate aerogels. *J. Sol-Gel Sci. Technol.* **1994**, *1*, 241–249. [[CrossRef](#)]
81. Livraghi, S.; Paganini, M.C.; Giamello, E.; Selloni, A.; Di Valentin, C.; Pacchioni, G. Origin of photoactivity of nitrogen-doped titanium dioxide under visible light. *JACS* **2006**, *128*, 15666–15671. [[CrossRef](#)] [[PubMed](#)]
82. Serpone, N. Is the band gap of pristine TiO₂ narrowed by anion-and cation-doping of titanium dioxide in second-generation photocatalysts? *J. Phys. Chem. B* **2006**, *110*, 24287–24293. [[CrossRef](#)] [[PubMed](#)]
83. Bahruji, H.; Bowker, M.; Davies, P.R.; Pedrono, F. New insights into the mechanism of photocatalytic reforming on Pd/TiO₂. *Appl. Catal. B* **2011**, *107*, 205–209. [[CrossRef](#)]
84. Marin, R.P.; Ishikawa, S.; Bahruji, H.; Shaw, G.; Kondrat, S.A.; Miedziak, P.J.; Morgan, D.J.; Taylor, S.H.; Bartley, J.K.; Edwards, J.K. Supercritical antisolvent precipitation of TiO₂ with tailored anatase/rutile composition for applications in redox catalysis and photocatalysis. *Appl. Catal. A* **2015**, *504*, 62–73. [[CrossRef](#)]
85. Fort, C.; Pap, Z.; Indrea, E.; Baia, L.; Danciu, V.; Popa, M. Pt/N-TiO₂ Aerogel composites used for hydrogen production via photocatalysis process. *Catal. Lett.* **2014**, *144*, 1955–1961. [[CrossRef](#)]
86. Holmen, A. Direct conversion of methane to fuels and chemicals. *Catal. Today* **2009**, *142*, 2–8. [[CrossRef](#)]
87. Müller, C.; Maciejewski, M.; Mallat, T.; Baiker, A. Organically modified titania-silica aerogels for the epoxidation of olefins and allylic alcohols. *J. Catal.* **1999**, *184*, 280–293. [[CrossRef](#)]
88. Müller, C.; Deck, R.; Mallat, T.; Baiker, A. Hydrophobic titania-silica aerogels: Epoxidation of cyclic compounds. *Top. Catal.* **2000**, *11*, 369–378. [[CrossRef](#)]
89. Coles, M.P.; Lugmair, C.G.; Terry, K.W.; Tilley, T.D. Titania-silica materials from the molecular precursor Ti[OSi(OtBu)₃]₄: Selective epoxidation catalysts. *Chem. Mater.* **2000**, *12*, 122–131. [[CrossRef](#)]
90. Choi, J.; Suh, D.J. Complete oxidation of 1, 2-dichlorobenzene over V₂O₅-TiO₂ and MnO_x-TiO₂ aerogels. *Korean J. Chem. Eng.* **2014**, *31*, 1773–1779. [[CrossRef](#)]
91. Kang, M.; Choi, J.; Kim, Y.T.; Park, E.D.; Shin, C.B.; Suh, D.J.; Yie, J.E. Effects of preparation methods for V₂O₅-TiO₂ aerogel catalysts on the selective catalytic reduction of NO with NH₃. *Korean J. Chem. Eng.* **2009**, *26*, 884–889. [[CrossRef](#)]

92. Kim, M.; Park, D.; Park, S.; Yang, X.; Choi, J.; Suh, D. Selective oxidation of hydrogen sulfide containing excess water and ammonia over vanadia-titania aerogel catalysts. *Catal. Today* **2006**, *111*, 212–216. [[CrossRef](#)]
93. Trueba, M.; Trasatti, S.P. γ -Alumina as a support for catalysts: A review of fundamental aspects. *Eur. J. Inorg. Chem.* **2005**, *2005*, 3393–3403. [[CrossRef](#)]
94. Matsuda, S.; Kato, A. Titanium oxide based catalysts—a review. *Appl. Catal.* **1983**, *8*, 149–165. [[CrossRef](#)]
95. Huirache-Acuña, R.; Nava, R.; Peza-Ledesma, C.L.; Lara-Romero, J.; Alonso-Núñez, G.; Pawelec, B.; Rivera-Muñoz, E.M. SBA-15 mesoporous silica as catalytic support for hydrodesulfurization catalysts—review. *Materials* **2013**, *6*, 4139–4167. [[CrossRef](#)] [[PubMed](#)]
96. Davis, K. Material review: Alumina (Al_2O_3). *Sch. Dr. Stud. Eur. Union J.* **2010**, *2*, 109–114.
97. Sui, R.; Rizkalla, A.S.; Charpentier, P.A. Formation of titania nanofibers: A direct sol-gel route in supercritical CO_2 . *Langmuir* **2005**, *21*, 6150–6153. [[CrossRef](#)] [[PubMed](#)]
98. Pakhare, D.; Spivey, J. A review of dry (CO_2) reforming of methane over noble metal catalysts. *Chem. Soc. Rev.* **2014**, *43*, 7813–7837. [[CrossRef](#)] [[PubMed](#)]
99. Kim, J.-H.; Suh, D.J.; Park, T.-J.; Kim, K.-L. Effect of metal particle size on coking during CO_2 reforming of CH_4 over Ni-alumina aerogel catalysts. *Appl. Catal. A* **2000**, *197*, 191–200. [[CrossRef](#)]
100. Bang, Y.; Seo, J.G.; Youn, M.H.; Song, I.K. Hydrogen production by steam reforming of liquefied natural gas (LNG) over mesoporous Ni- Al_2O_3 aerogel catalyst prepared by a single-step epoxide-driven sol-gel method. *Int. J. Hydrogen Energy* **2012**, *37*, 1436–1443. [[CrossRef](#)]
101. Bang, Y.; Seo, J.G.; Song, I.K. Hydrogen production by steam reforming of liquefied natural gas (LNG) over mesoporous Ni-La- Al_2O_3 aerogel catalysts: Effect of La content. *Int. J. Hydrogen Energy* **2011**, *36*, 8307–8315. [[CrossRef](#)]
102. Seo, J.G.; Youn, M.H.; Bang, Y.; Song, I.K. Hydrogen production by steam reforming of simulated liquefied natural gas (LNG) over mesoporous nickel-M-alumina (M = Ni, Ce, La, Y, Cs, Fe, Co, and Mg) aerogel catalysts. *Int. J. Hydrogen Energy* **2011**, *36*, 3505–3514. [[CrossRef](#)]
103. Yoo, J.; Bang, Y.; Han, S.J.; Park, S.; Song, J.H.; Song, I.K. Hydrogen production by tri-reforming of methane over nickel-alumina aerogel catalyst. *J. Mol. Catal. A: Chem.* **2015**, *410*, 74–80. [[CrossRef](#)]
104. Han, S.J.; Bang, Y.; Yoo, J.; Seo, J.G.; Song, I.K. Hydrogen production by steam reforming of ethanol over mesoporous Ni- Al_2O_3 - ZrO_2 xerogel catalysts: Effect of nickel content. *Int. J. Hydrogen Energy* **2013**, *38*, 8285–8292. [[CrossRef](#)]
105. Song, J.H.; Han, S.J.; Yoo, J.; Park, S.; Kim, D.H.; Song, I.K. Hydrogen production by steam reforming of ethanol over Ni-Sr- Al_2O_3 - ZrO_2 aerogel catalyst. *J. Mol. Catal. A Chem.* **2016**, *424*, 342–350. [[CrossRef](#)]
106. Lee, S.-H.; Suh, D.J.; Park, T.-J.; Kim, K.-L. The effect of heat treatment conditions on the textural and catalytic properties of nickel-titania composite aerogel catalysts. *Catal. Commun.* **2002**, *3*, 441–447. [[CrossRef](#)]
107. Krompiec, S.; Mrowiec-Białoń, J.; Skutil, K.; Dukowicz, A.; Pająk, L.; Jarzębski, A. Nickel-alumina composite aerogel catalysts with a high nickel load: A novel fast sol-gel synthesis procedure and screening of catalytic properties. *J. Non-Cryst. Solids* **2003**, *315*, 297–303. [[CrossRef](#)]



© 2018 by the authors. Licensee MDPI, Basel, Switzerland. This article is an open access article distributed under the terms and conditions of the Creative Commons Attribution (CC BY) license (<http://creativecommons.org/licenses/by/4.0/>).